universität
wien

DIPLOMARBEIT / DIPLOMA THESIS

Titel der Diplomarbeit / Title of the Diploma Thesis

„ Evaluation of multi-colour transfections via flow cytometry "

verfasst von / submitted by

Islam Abd El Rahman

angestrebter akademischer Grad / in partial fulfilment of the requirements for the degree of

Magister der Pharmazie (Mag. pharm.)

Wien, 2017 / Vienna, 2017

Table of Contents

1 Introduction

Cancer is one of the leading causes of mortality worldwide with approximately 14.1 million new cases in 2012 and 8.2 million related deaths (Torre et al. 2015). According to "Statistik Austria", 39.000 new incidents are documented every year in Austria (Statistics Austria 2017). The case incidence is growing, as the average human life time is increasing (Cancer Research UK 2015). Therefore, the understanding of how cancer cells work is essential to gain more prevention and therapeutic methods to control this burden.

1.1 The acquired capabilities of cancer cells

Tumorigenesis is a multistep process that leads to a transformation of healthy human cells into malignant derivatives (Hanahan and Weinberg 2000). Research in the past decades established the dynamic changes in cancer cells (Hanahan and Weinberg 2000). In this process, the mutation of tumour suppressor genes and oncogenes are the fundament of the occurrence of a cancer cell (Bishop and Weinberg 1996). Six fundamental alterations in the cancer genotype are leading to an occurrence and retention of cancer (Figure 1).
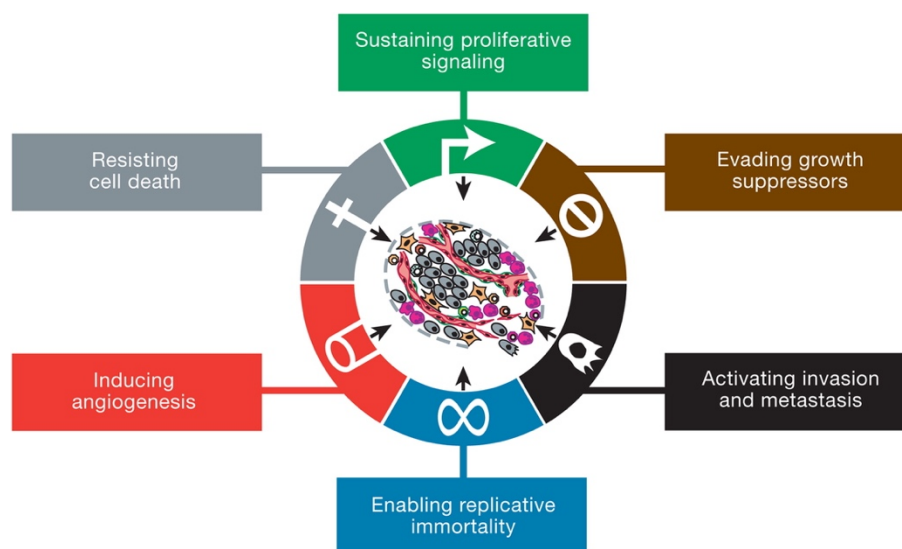
Figure 1 Hallmark capabilities of cancer
This figure suggested by Hanahan and Weinberg 2011 shows the characteristics that a cancer cell has to obtain for malignancy (figure from Hanahan and Weinberg 2011)

1.2 Cancer stem cells

Recent research has started to look at tumour tissue as an "own living organism", complete with its own self-organisation (Hanahan and Weinberg 2000; Kreso and Dick 2014). That means that similar as a healthy human organism, it depends on many factors to maintain survival. And as every living being undergoes small-scale evolution by mutation, so could cancer cells, as proposed in Nowell's work (Nowell 1976).

In healthy tissue, stem cells are crucial for maintenance of tissue homeostasis and repair (Beck and Blanpain 2013). Cell hierarchies, like already known in normal stem cells, for example in keratinocytes, which give rise to three types of colonies, may also be present in the Cancer Stem Cell (CSC) model (Barrandon and Green 1987). It has been demonstrated that not all tumour cells are the same and that within some cancers some tumour cells are more differentiated than others, which suggested that the undifferentiated tumour cells are the controversially discussed cancer stem cells (Pierce et al. 1959, 1960). They are defined as self-renewable cells and as cells with long-term repopulation capacity (Clarke et al. 2006; Nguyen et al. 2012). Their tumour-initiating or leukaemia-initiating character is crucial for its definition (Kreso and Dick 2014). Quintana's CSC studies were essential in demonstrating their existence (Quintana et al. 2008, 2010).

Cancer stem cells are connected to therapy resistance and disease progression (Hanahan and Weinberg 2011). An additional proposal is that quiescent CSCs could drift to distant places , and could be responsible for metastases (Clevers 2011).

Two models to explain the proliferation of cancer cells are usually proposed (Beck and Blanpain 2013). In the stochastic model, cells are considered equipotent, where every cell have the potential giving rise to a new tumour cell. In the hierarchic model, only certain cells provide long-term tumour growth (Beck and Blanpain 2013) (Figure 2). Both models are not to be treated separately, because a cancer cell may switch between these two states (Dick 2008).
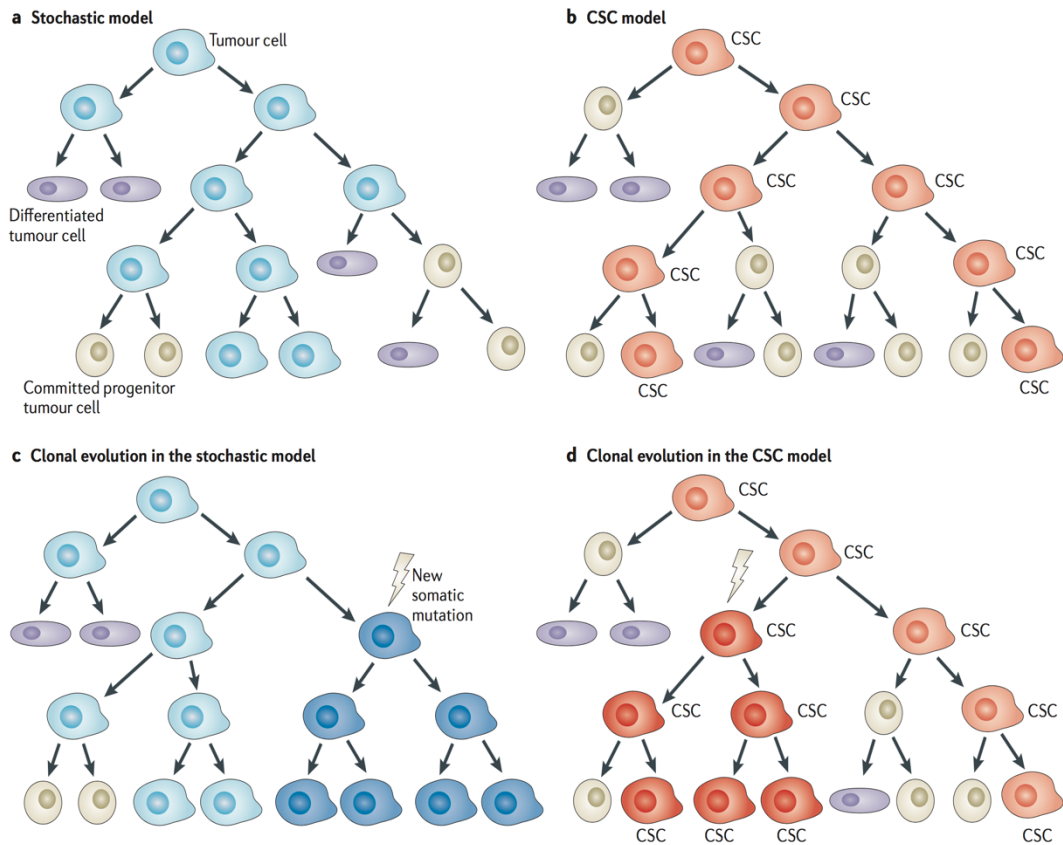
Figure 2 Comparison of the two usually proposed models of tumour growth. a | In the stochastic model, cells are equipotent. Every cell can give rise to a new tumour cell. Heterogeneity is a result of self-renewal and differentiation. **b** | In the CSC model only some cells have the ability for long-term self-renewal and these cells can also give rise to new tumour cells, which provides the tumour heterogeneity. **c, d** | In both models new mutations can lead to an increase of tumour heterogeneity (figure from Beck and Blanpain 2013).

1.2.1 Approaches to identify CSCs

Improved techniques have shown that some tumours have variations on the cell surface which can be used as markers (Pertschuk et al. 1978; Dexter et al. 1978; Raz et al. 1980; Poste et al. 1980). In connection with CSCs some surface markers are used for their identification such as CD34 which occurs in hematopoietic malignancies (Hope, Jin, and Dick 2004). In main projects the focus is set on developmental pathways (1.2.2) within cancer stem cells and so could lead us to more unambiguous results to define CSC.

1.2.2 Developmental signalling pathways in cancer stem cells

As more studies support the theory that the function of CSC depends on ligand-receptor mediated signalling pathways (Beachy et al. 2010, Amakye et al. 2013), the most extensively studied ones, i.e. Hedgehog, Notch and Wnt, are explained in the following section. These pathways are evolutionary conserved and represent cell-fate-determination-pathways. They are indispensable in the research of cancer biology as they are non only involved in CSC biology, but also angiogenesis, carcinogenesis and tumour maintenance (Espinoza and Miele 2013).

The Hedgehog (HH) pathway (Figure 3)

The HH pathway is mainly involved in the patterning of tissue during embryonic development, the repair of normal tissues and in the transition from an epithelial to a mesenchymal cell type (Beachy et al. 2010). Furthermore, it plays a role in the development of sebaceous glands (Athar et al. 2006), as well as in embryonal and adult brain development (Palma et al. 2005), in proliferation, survival and angiogenesis (Amakye et al. 2013). Relevant ligands which activate the HH pathways are Sonic hedgehog (SHH), Indian hedgehog (IHH) and Desert hedgehog (DHH). They act by binding to the patched transmembrane receptors (PTCH) and so inhibits the effect on the also membrane located Smoothened (SMO)(Odoux et al. 2008). As a result, SMO activates GLI transcription factors, which get localized into the nucleus leading to the expression of HH target genes.

Therapeutic approaches targeting the HH Pathway

Robotnikinin, a small molecule that binds SHH and blocks HH signalling in human cells, represents a potential therapeutic approach (Stanton et al. 2009). By its binding on SHH an activation of SMO is inhibited, which result in blocking the following downstream processes (Figure 3). Approved therapeutics, such as the SMO antagonists Vismodegib and Sonidegib, that directly act on SMO are already used in the clinics to treat basal cell carcinoma (FDA, 2013). The clinical trial on Saridegib was stopped in phase 2 because of its similarity to placebo ('Infinity Stops Phase 2 Trials of Saridegib in Chondrosarcoma and Myelofibrosis' 2012)
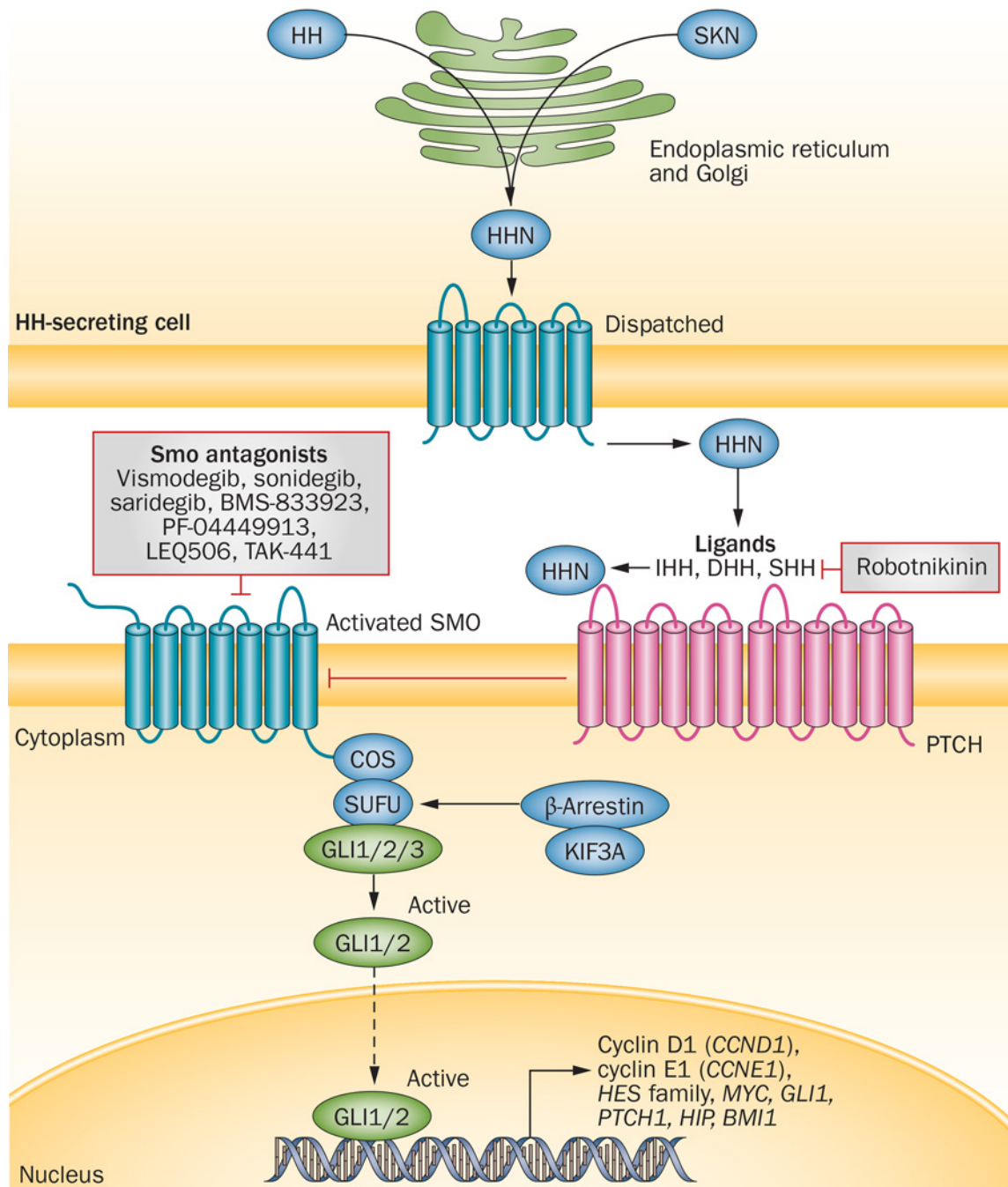
Figure 3 The Hedgehog pathway. In the "off" state, PTCH inhibits SMO activity. Once Hedgehog (HH) ligands, Indian hedgehog (IHH), Desert Hedgehog (DHH) or Sonic hedgehog (SHH) are released, the proteins bind on Patched (PTCH) resulting in loss of inhibitory action towards Smoothened (SMO). Withhin the downstream processes, several proteins get activated, which in turn leads to an activation of GLI. GLI acts as transcription factor, regulating the expression of HH targeted genes. Vismodegib and Sonidegib are approved SMO antagonists. Robotnikinin has potential for a therapeutic approach. (figure from Takebe et al. 2013) | Abbreviations: COS, Costal; DHH, Desert hedgehog; HH, Hedgehog; HHC, Hedgehog *C*-terminal domain; HHN, Hedgehog *N*-terminal domain; HIP, Hedgehog interacting protein; IHH, Indian hedgehog; Ptch, Patched; SHH, Sonic hedgehog; SKN, Skinny hedgehog; SMO, Smoothened; SUFU, suppressor of fused

9

The Notch pathway (Figure 4)

The Notch signalling pathway is rather complex, as it comprises five approved Notch ligands (Delta-like ligand 1, 3 and 4 [DLL1, 3 and 4], and Jagged1 and 2), and four receptors (Notch 1-4) (Gu et al. 2012) that can differ in different tumours and tumour subtypes (Takebe et al. 2015). For Notch signalling, at least two neighbouring cells are required, a signal-sending and a signal-receiving cell (Gómez-del Arco et al. 2010). Both, ligands and receptors are directly integrated into the cell membrane of the respective cell (Gómez-del Arco et al. 2010). The Notch receptor contains an extracellular domain with EGF-like repeats, which are involved in ligand binding, and an intracellular domain (ICD) (Karamboulas and Ailles 2013). The cell-to-cell interaction leads to two proteolytic reactions performed by a disintegrin and metalloprotease (ADAM protease) in the first step, and the γ-secretase complex, composed of four units called Niscastrin, Presenelin, APH-1 and APH-2, in the second step (Takebe et al. 2015). Consequently, an active intracellular domain, NICD is released (Karamboulas and Ailles 2013). NICD is consequently translocated into the nucleus and leads to related gene expressions which regulate central cell-fate choices, including differentiation, cell-cycle progression and survival.

Therapeutic approaches targeting the Notch Pathway

Some potential therapeutic inhibitors of the Notch signalling pathway are discussed. An option is to inhibit the pathway activity at the receptor level: there the mechanism of action is similar to the one known for TNFα blockers, like Etanercept or Infliximab (Gardam et al. 2003). These biologicals are structurally related to the physiological TNFα receptors and so can bind TNFα. Similarly, the use of decoy receptors binding to Notch ligands could be an interesting approach. Another option is the development of monoclonal antibodies (mAbs) targeting both notch ligands and receptors. Also in the clinical pipeline are mAbs or small molecules to nicastrin, a component of the γ-secretase complex (Takebe et al. 2015)
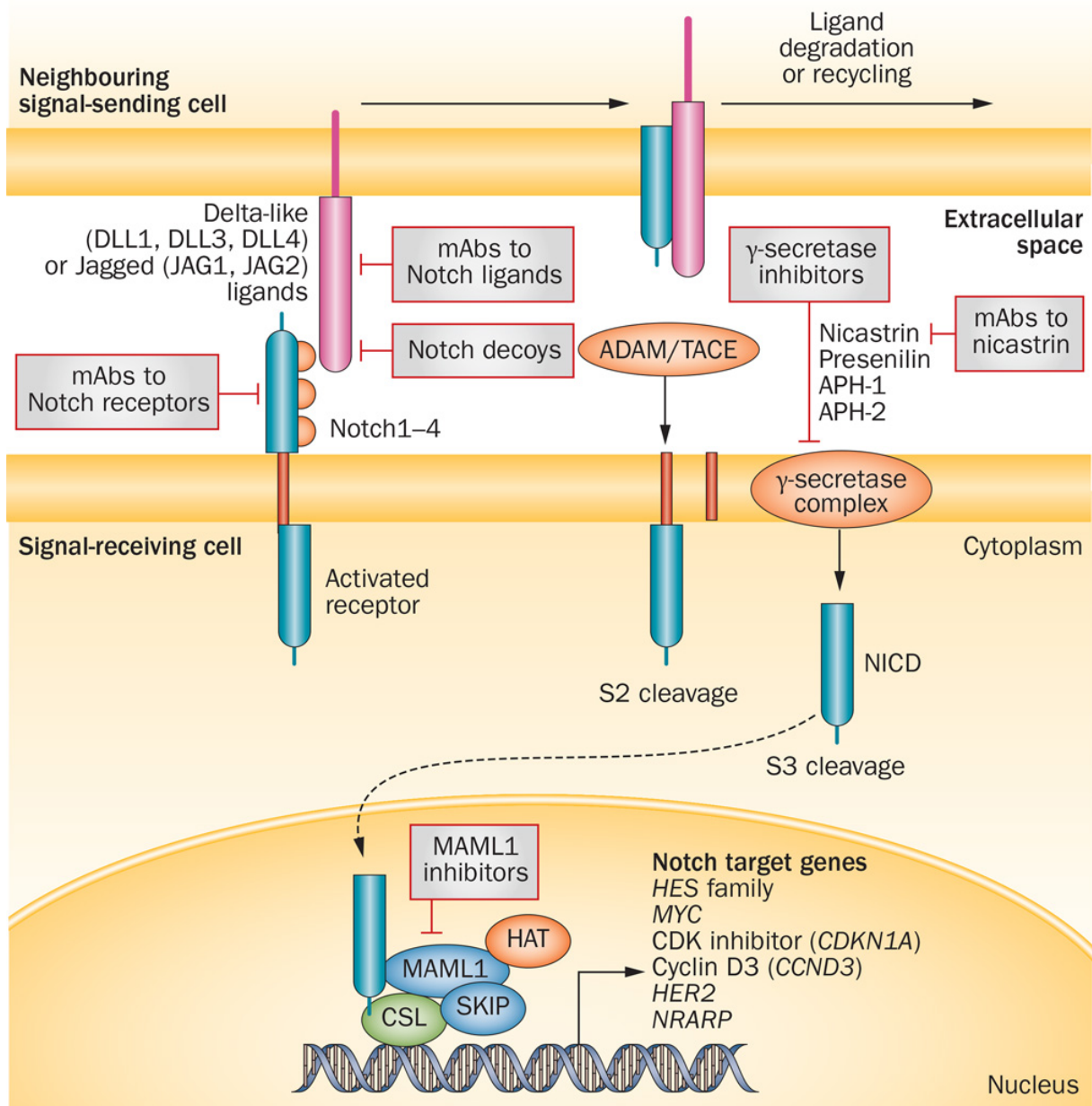
Figure 4 The canonical Notch signalling pathway. Transmembrane Delta-like (DLL1, DLL3, DLL4) or Jagged ligands (JAG1, JAG2) of the signal-sending cell interact with the Notch receptors of the signal-receiving cell. This cell-to-cell interaction leads to two proteolytic reactions performed by a disintegrin and metalloprotease (ADAM protease) in the first step, and a γ-secretase complex in the second step. This leads to an activation of the Notch intracellular domain (NICD), and through its translocation into the nucleus, activates a Notch related gene-expression. Among these are genes with central roles in cell-fate choices. (figure from Takebe et al. 2015) | Abbreviations: ADAM, a disintegrin and metalloproteinase; APH-1/2, anterior pharynx-defective-1/2; CSL, CBF1/Su(H)/Lag-1; DLL, delta-like ligand; HAT, histone acetyltransferase; HES, hairy and enhancer of split-1; JAG1, Jagged-1; JAG2, Jagged-2; mAb, monoclonal antibody; MAML1, Mastermind-like 1; NICD, Notch intracellular domain; NRARP, Notch-regulated ankyrin-repeated protein; SKIP, ski-interacting protein; TACE, TNF-α-converting enzyme (also known as ADAM17).

The Wnt Pathway (Figure 5)

Three pathways for Wnt signalling are described so far (Takebe et al. 2015) with the canonical Wnt pathway being the most relevant (Takebe et al. 2015), which will be focused on here. Wnt ligands bind to a G-protein-coupled receptor complex. This complex consists of Frizzled and a co-receptor, a low density lipoprotein receptor-related protein 5/6 (LRP5/6) (Takebe et al. 2015). This leads to activating of the protein dishevelled homologue (Dvl) phosphoprotein (Gao and Chen 2010). Dvl inhibits a multiprotein destruction complex that contains Axin. Axin-mediated β-catenin phosphorylation is now inhibited, resulting in accumulation of cytoplasmic β-catenin (Habas and Dawid 2005). By this accumulation β-catenin is translocated into the nucleus, where it activates its target genes in conjunction which TCF-LEF transcription factors. In the absence of wnt ligand, β-catenin is degraded by a multiprotein destruction complex (Figure 5) while Wnt signalling remains inactive (Behrens 2000).
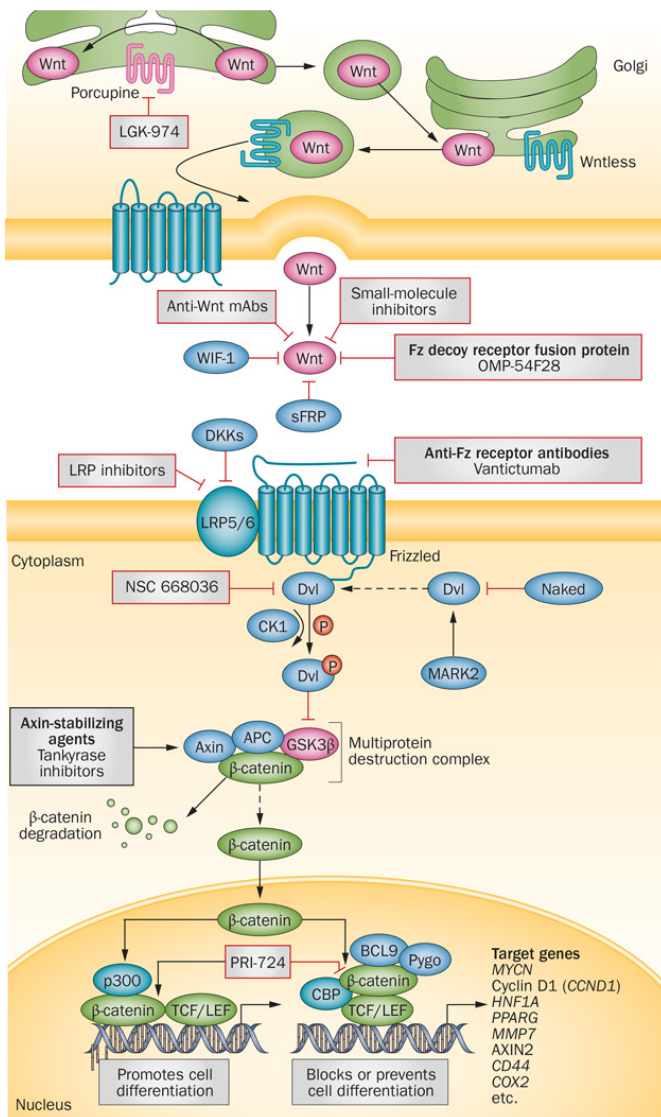
Figure 5 The canonical Wnt signalling pathway and potential intervention points. Porcupine and Wntless are two proteins among others which regulate the secretion of Wnt proteins. LGK-974, a small molecule in phase 1 study, targets Porcupine and so inhibits Wnt ligand secretion. Binding of wnt ligands to their receptor complex results in intracellular accumulation of β-catenin. This happens because of a Dvl mediated destruction of the multiprotein destruction complex. Sulindac, a NSAID targets Dvl. In the absence of Wnt signalling this complex otherwise degrades β-catenin. As a final step of this cell signalling cascade β-catenin is translocated into the nucleus leading to Wnt related gene expression. (figure from Takebe et al. 2015) | Abbreviations: APC, adenomatous polyposis coli protein; BCL9, B-cell lymphoma 9; CBP, cyclic AMP response element-binding protein; CK1, casein kinase 1; DKKs, dickkopfs; Dvl, Dishevelled; Fz, Frizzled; GSK3β, glycogen synthase kinase 3β; LRP5/6, low-density lipoprotein receptor-related protein 5/6; mAbs, monoclonal antibodies; PPARG, peroxisome proliferator-activated receptorγ;Pygo,Pygopus;sFRP,secretedFrizzled-related protein; TCF/LEF, T-cell-specific transcription factor/lymphoid enhancer-binding factor; WIF-1, Wnt inhibitory factor 1.

Some Wnt-pathway inhibitors are under investigation whereas other approved and therefore already on the market.

Sulindac, approved by the FDA is available as a NSAID. It shows action in breast cancer inhibition by acting as an immune modulator (Yin et al. 2016). Another mechanism of action is discussed. It is proposed that Sulindac inhibits the canonical Wnt pathway by blocking a specific domain of the protein Dvl (Lee et al. 2009).

Other agents under preclinical investigation are Tankyrase Inhibitors, which act by stabilizing Axin. (Huang et al. 2009). Tankyrase itself is responsible for the proteosomal degradation of Axin (Waaler et al. 2012).

Monoclonal antibodies interrupting Wnt signalling are also investigated. They are divided in two groups: those that neutralize Wnt ligands, and those that inhibit the Wnt receptors Fz, like Vantictumab (Smith et al. 2013) and LRP. OMP-54F28 represents a decoy receptor under investigaton (Takebe et al. 2015). It could be shown that it decreases CSC numbers in patient-derived tumour growth (Smith et al. 2013).

The importance of understanding these three pathways in detail is helpful for understanding the occurrence and maintenance of cancer. Visualisation methods are our approach for that. Pathways activity within a tumour could show in how far they are playing a role in the incurrence of cancer. In associated projects attention is payed in how to visualize these pathways via fluorophores to eventually better understand these pathways and make them analytically graspable. In this project, the choice of these fluorophores is relevant.

1.3 Fluorescent reporter proteins

The history of the usage of fluorescent proteins began just when the original *Aequorea victoria* jellyfish wild-type green fluorescent protein (GFP) was used to highlight sensory neurons in the nematode (Chalfie et al. 1994). Since then, researchers of this field are focusing on production and finding of new and improved versions of this protein that are brighter, cover a broad spectral range and show enhanced photostability (Shaner et al.

2007). The wild type (wtGFP) was quickly modified to produce variants emitting in the blue (blue fluorescent protein - BFP), cyan (cyan fluorescent protein - CFP) and yellow (yellow fluorescent protein - YFP) regions (Heim et al. 1994; Ormo et al. 1996; Tsien 1998). The orange and red spectral regions have emerged as a challenge with alterations of *Aequorea* GFP until the discovery of the first red FP from a non- bioluminescent reef coral (Matz et al. 1999). This was considered as another revolutionary breakthrough as a a bright and photostable monomeric red-emitting derivative, whose performance is similar of that of the best GFP variants had been discovered (Shaner et al. 2007). In the following the fluorescent reporter proteins used in our experiments are introduced:

EGFP (Enhanced Green Fluorescent Protein, Figure 6): Excitation maximum: 488 nm, emission maximum: 507 nm (Shaner et al. 2005). In just a few years, the green fluorescent protein (GFP) from the jellyfish *Aequorea Victoria* (Shimomura et al. 1962) became one of the most widely studied proteins in biochemistry and cell biology (Tsien 1998). It shows an amazing ability to generate a highly visible fluorescence (Tsien 1998). GFP is well established as a marker of gene expression and protein targeting in intact cells and organisms (Tsien 1998). EGFP is a stability improved (Shaner et al. 2005), red shifted version of GFP. The mutation resulting in EGFP was developed by Cormack with the purpose to optimize it for flow cytometry analysis (Cormack et al. 1996).
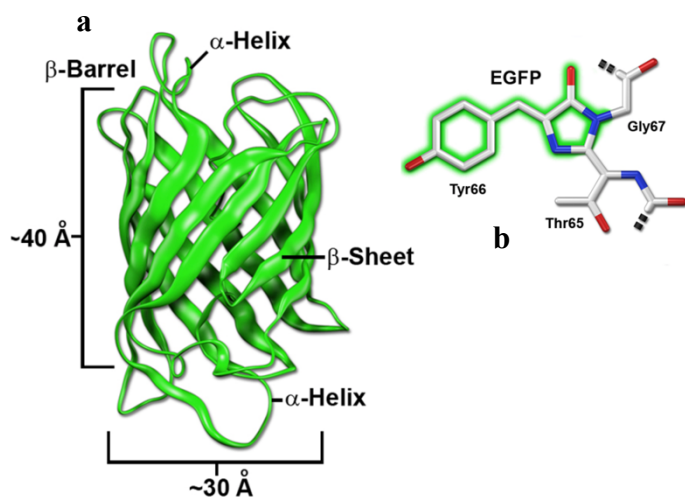
Figure 6 a | Fluorescent reporter protein barrel architecture and approximate dimensions, and chromophore structures of common *Aequorea* FP derivatives. **b** | EGFP: chromophore that is conjugated and is responsible for fluorescence is shaded green. (Figure from Shaner et al. 2007)

iRFP713 (near Infrared Fluorescent Protein): Excitation maximum: 690 nm, emission maximum: 713 nm (Lecoq and Schnitzer 2011). It was bioengineered by multiple mutagenesis of a phytochrome from the bacterium *Rhodopseudomonas palustris* and so improved in its protein properties (Filonov et al. 2011). IRFP exhibits good properties (Lecoq

and Schnitzer 2011) for analysis in tissues and for *in vivo* imaging. Physiological biliverdin levels seemingly fully activate iRFP fluorescence (Lecoq and Schnitzer 2011).

mT2 (mTurquoise2): Excitation maximum: 434 nm, emission maximum: 474 nm (Goedhart et al. 2012). The popular, but barely bright, Enhanced Cyan Fluorescent Protein (ECFP) was improved into brighter variants (Goedhart et al. 2012). Among these variants mTurquoise is one that shows high fluorescence characteristics and long lifetime (Goedhart et al. 2012). Thanks to structural analysis and following mutations related to amino acid 146 (Phe instead of Ile) mTurquoise could be enhanced and mTurquoise2 (mT2) was born (Figure 7). mTurquoise2 exhibits a high-fluorescent yield and has mono-exponential fluorescence lifetime (Goedhart et al. 2012). Additionally it shows high increase in stabilization of the chromophore(Goedhart et al. 2012), which is explained in Figure 7. These characteristics made mT2 a preferable fluorescent reporter protein in respect of our experiments.
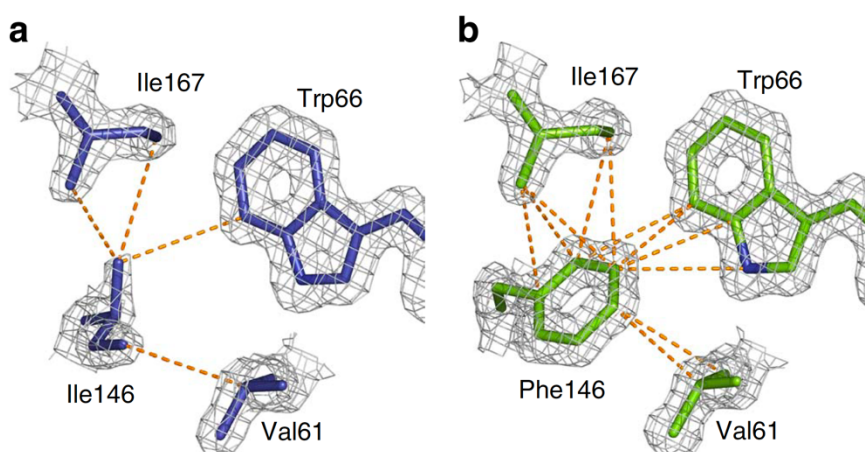
Figure 7 Structural comparison of mTurquoise and mTurquoise2. **a** | Environment of residue 146 (Isoleucine) in mTurquoise and **b** | in mTurquoise2 (Phenylalanine). Inter-atomic distances lower than 4.0 Å, characteristic of Van der Waals (VdW) interactions, are represented as dotted orange lines. The much greater number of such distances in mTurquoise2 illustrates the marked increase in stabilization of the chromophore by vdW interactions. (Figure from Goedhart et al. 2012)

tdTomato (Tandem Dimer Tomato): Excitation maximum: 554 nm, emission maximum: 581 nm (Shaner et al. 2005). Tdtomato, which is a protein dimer in its quaternary structure is originally derived from DsRed firstly found in *Discosoma* sp (Shaner et al. 2004) It shows a very high brightness when excited. (Shaner et al. 2005).

The use of fluorescent reporter proteins is a well established method to gather information on the activity of certain signalling pathways. In associated projects this method should be used to visualize the three developmental pathways. The fluorophores EGFP , iRFP, tdTomato and mTurquoise2 were utilized in this thesis (see Discussion). We've chosen these four fluorophore reporter proteins because they fit to the excitations lasers and emission filters of our flow cytometer by Miltenyi (MACSQuant® Analyzer 10) and furthermore have a wide excitation and emission spectrum. We also want a broad range of fluorescent proteins for other experiments in our laboratories. The fluorescent reporter proteins were expressed via pathway related promotors. To standardise the experiment, we've used the CMV promotor for every fluorophore expression. Testing how these fluorescent reporter proteins perform in our flow cytometer represents the core of this thesis. The reason why fluorescent reporter proteins are tested and no other fluorescent compounds like reactive or conjugated dyes is the fact that protein expression allows us to get clues about promotor activities and so allows us to conduct promotor studies.

Noteworthy are the requirements of fluorophores in analytical experiments:

1. Fluorophores shouldn't intoxicate cells (Shaner et al. 2005)
2. Strong and long brightness to be easy detectable (Shaner et al. 2005)
3. In cases were more fluorophores are used: very low interferences (Shaner et al. 2005)

The plasmid reporter construct that contains the genetic information of all fluorophores mentioned above – 3P – TOP:

In addition to the four fluorophores we've also used the so called 3P-TOP plasmid in our experiments. It contains wnt, notch or hedgehog-sensitive promotors for each previously described fluorophore (recently developed by Julia Maier in the course of her PhD work). This construct is relevant for other associated projects by Julia Maier.

Table 1 summarises the properties of excitation and emission of the fluorophores used in experiments:

Table 1 Properties of the used fluorophores

Fluorophore	Excitation$_{max}$ (nm)	Emission$_{max}$ (nm)
EGFP	488	507
iRFP	690	713

mT2	434	473
tdTomato	554	581

1.3.1 Insight into our flow cytometer and spectral overlap compensation of fluorescent reporter proteins and its challenges

When the light emitted from one fluorophore emits into the detector which measures the signal emitted by another fluorophore signal overlap occurs. The consequences for research are false positive signals. It is possible to eliminate this by electronically removing this signal by a process called compensation. The concept of compensation continuous to be one of the aspects of flow cytometry which is confusing although many instruments and software packages can perform automatic compensation for researchers it is still important to understand the basic principle. Compensation is a process by which spill over fluorescence is removed from secondary parameters so that the fluorescence values for a parameter reflect only the fluorescence of the primary fluorophore. In a perfect world, the fluorescence emission profile for each individual fluorophore would be very intense and separated well from the other emission peaks (Figure 8A). In reality however fluorophores have broader emission peaks as shown in the emission profile of Alexa Fluorophore 488 and R-PE (Figure 8B). In this case researchers need to be sure that fluorescent emission recorded from Alexa dye is coming from the Alexa dye and not from RPE. Here compensation becomes relevant. Therefore a correction of the emission signal is needed. In multiparameter
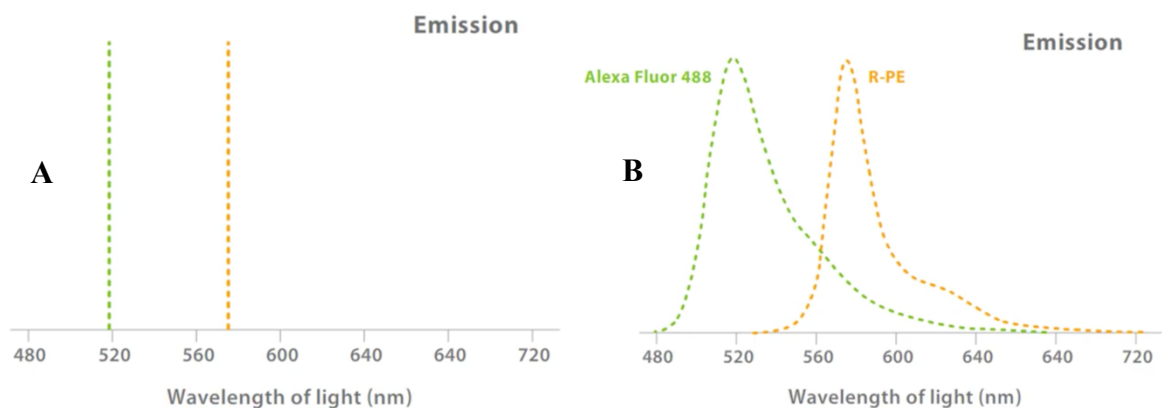
Figure 8 A | Perfect, but unrealistic emission signal vs. **B |** broad emission peaks that can sometimes overlap in multicolour experiments shown in emission signals of Alexa Fluorophore and R-PE (figures from Thermo Fischer Scientifics webinar, "Basics of flow cytometry")

17

experiments the flow cytometer records fluorescence using an emission filter chosen to collect the maximum amount of light from one fluorophore of interest and to exclude much light as possible from the other fluorescence reporter protein in our case. In figure 9 Alexa fluorophore emission is corrected with a 530 nm filter and R-PE corrected with a 585 nm filter. Alexa emission overlap into the R-PE spectra requires more compensation than the R-PE into Alexa overlap (Figure 9, shown in red).
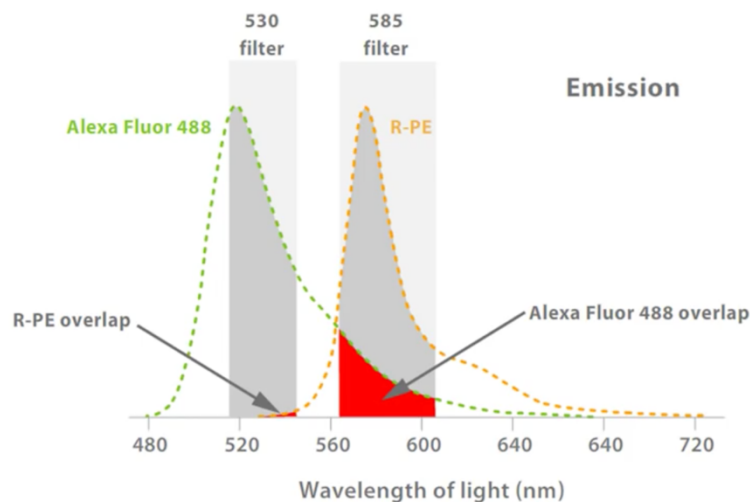
Figure 9 Example of spectral overlap shown in emission spectra of Alexa Fluorophore 488 and R-PE. (figures from Thermo Fischer Scientifics webinar, "Basics of flow cytometry").

The suited optical filter configuration (Table 10) and real-time electronic devices or post analysis software-based (e.g. FlowJo X, www.flowjo.com, Ashland, Oregon, USA, what is commonly used in our laboratory) compensation provide the possibility to differ between a broad range of different fluorescent reporter proteins with partially overlapping light spectra (Hawley et al. 2004). Some flow cytometers are featured with inter-laser compensation electronic circuitry and thus the generation of a compensation matrix during data acquisition is possible. For flow cytometers not equipped with inter-laser compensation electronic circuitry, software post-acquisition compensation is the only option.

Due to overlapping excitation spectra, some fluorescent reporter proteins can be excited by a single excitation laser and this had even been shown in Beavis studies where yellow and green fluorescent proteins have been tested by using the same excitation wavelength (Beavis and Kalejta 1999). Many commercial flow cytometers are featured with lasers with fixed excitation wavelengths (Hawley et al. 2004). Our flow cytometer is equipped with

405, 488 and 635 nm excitation lasers. Additionally, our flow cytometer has 10 optical channels for multiparameter flow cytometry and so allows a simultaneous detection of emission signals. Measurements of signals in flow cytometry are based on two intensity depended and symmetric mechanisms: 1) photon counting (counting errors) and 2) conversion from analogue-to-digital (conversion or digital errors) (Hawley et al. 2004). Compensation as a subtractive process results to fine but important problems like having negative computed values for some events (Hawley et al. 2004). This behaviour gets evident when the measurement is transformed and displayed as log data: negative and zero channel values are normally set to 1, as the log function is undefined at less than or equal to 0 (Hawley et al. 2004). This data reduction has at least two undesirable consequences:

1. The data are plotted on the axis and are not easily visualized in the display (Hawley et al. 2004).
2. The variability is no longer symmetric and, as a result, the data appear to be under-compensated (Hawley et al. 2004). (Figure 10, row 7)

Figure 10 demonstrates flow cytometry data where compensation have been used. These data are provided from Hawleys work (Hawley et al. 2004). In this work, fluorescent reporter plasmids transfection experiments are performed in Sp2/0-Ag14 cells. Cells were transfected with retroviral vectors carrying the ECFP (Enhanced Cyan –FP), EGFP, EYFP (Enhanced Yellow –FP) or DsRed fluorescent protein gene.

In this context, when we demonstrate in how far our tested fluorescent reporter proteins overlap in their spectra we could accomplish a compensation matrix. Our flow cytometer is featured with the capability of establishing compensation matrixes and therefore can used as part of other projects regarding fluorophore compensation.
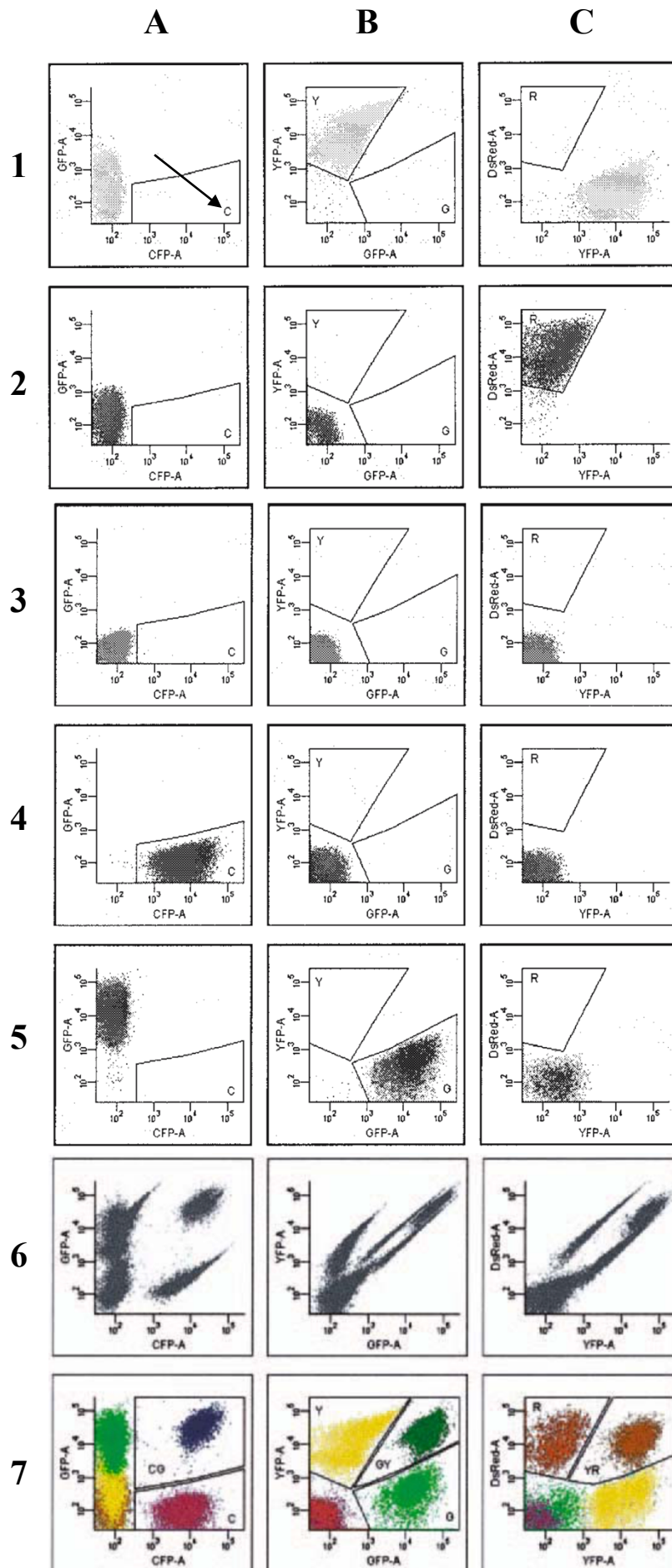
Figure 10. 1 | Bivariate histograms demonstrating detection of untreated Sp2/0-Ag14 cells, **2** | Sp2/0-Ag14 cells expressing ECFP, **3** | EGFP, **4** | EYFP, or **5** | DsRed using 488-nm and 407-nm excitation. This data was acquired and analyzed by Hawley et al. using FACSDiVa software. It calculated spectral overlap among all parameters and compensated these values after acquisition. Areas named C = ECFP-positive (shown with an arrow), G = EGFP-positive, Y = EYFP-positive and R = DsRed-positive (from left to right), where marked by using no rectilinear markers. A mixture of Sp2/0-Ag14 cells, cells expressing the individual fluorescent proteins and cells expressing all four fluorescent proteins is shown **6** | before and **7** | after spectral overlap compensation. the first three plots (from left to right in row 7) represent ECFP/EGFP-positive, EGFP/EYFP-positive, and EYFP/DsRed- positive cells respectively marked as "CG," "GY," and "YR". (figure from Hawley et al. 2004).

1.4 Transfection

Gene delivery methods are promising in the field of gene therapy (Jin et al. 2014). Viral, physical and chemical methods are the major ways for gene transfer. We used *in vitro* transfection of A549 lung cancer cells with a chemical method. In our laboratory, we have used linear polyethylenimine (LPEI) as a cationic polymer (Figure 11) as gene delivery agent. It is supplied in our laboratory by Alexander Taschauer (University of Vienna, MMCT).
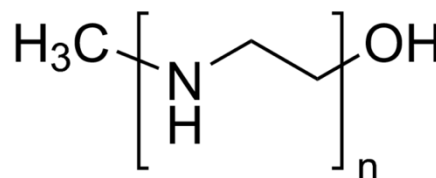
Figure 11 Chemical structure of LPEI | In our experiments LPEI with a molecular weight of 10kDA was used

Cationic polymers promise a safe, and convenient alternative to viral gene delivery vectors, relying on endocytosis of particles formed with nucleic acids by the virtue of electrostatic interaction (Schaffert et al. 2012; Zhang et al. 2013). These gene delivery particles are called *polyplexes* (Jin et al. 2014). Polyethylenimines (PEI) are the most investigated among various kinds of cationic polymers because its outstanding properties (Jin et al. 2014):

1. It shows a strong DNA condensation capacity (Jin et al. 2014)
2. It exhibits intrinsic endosomolytic activity (Jin et al. 2014)
3. It has a unique buffering capacity known as proton sponge effect (Figure 12B) (Jin et al. 2014)

Figure 12 summarizes how LPEI acts as a delivery system and unfolds its unique properties.

As shown in figure 12B the proton sponge effect facilitate the endosomal escape of the DNA via osmotic swelling and burst of the endosome (Brown et al 2001; De Laporte, Rea, and Shea 2006).

The transfection efficiency depends on the ratio of LPEI and DNA, the N/P ratio used. (Nimesh et al. 2007; Vu et al. 2012). N stands for the Amino Nitrogen in LPEI and P for the Phosphate groups in the DNA. N/P ratios higher than 3 enable an excess of free LPEI which is connected to the endosomal escape (Boeckle et al. 2004) . This also explains the usually enhanced transfection efficiencies at higher N/P ratios. Additionally, the efficiency of polyplexes highly depends on the molecular weight of LPEI (Jin et al. 2014). The experience in our laboratory showed that 10kDa LPEI allows satisfying transfection experiments. Thanks to the high density of positive charge, high-molecular LPEI can condense DNA in an effective way and so form nanometre sized particles easily being endocytosed (Dunlap et al. 1997). Still the usage of high molecular LPEI is challenging as it can form not degradable toxic linkages like C-C or C-N bonds responsible for acute cytotoxicity due to cell membrane disruption followed by apoptosis (Moghimi et al. 2005; Kawakami et al. 2006). Low molecular weight LPEI, on the other side shows low cytotoxicity but an undesirable transfection efficiency (Godbey et al. 1999; Zou et al. 2000). Therefore, the preparing of polyplexes with high transfection efficiency and low cytotoxicity is challenging.
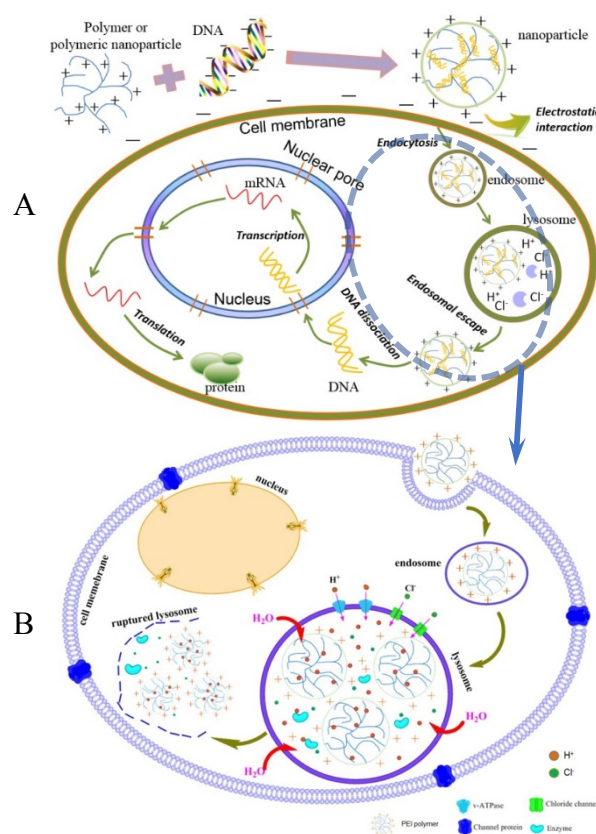
Figure 12 The unique properties of PEI as cationic DNA delivering system. A | Scheme shows how the DNA and cationic polymer complex is emerging and finally incorporated into the eukaryotic cell via endocytosis after an electrostatic interaction between the cationic PEI and the negatively loaded membrane. The amount that can escape into the cytosol is proportional to the PEI used. Once the polyplex is in the cytosol, the DNA dissociates and is finally incorporated by the nucleus ready to be transcribed. **B |** Schematic representation of the proton sponge effect: Through osmotic swelling and burst of endosomes the release of the gene is facilitated. (Fugure from Jin et al. 2014).

1.5 Competent cells

E. coli strains are routinely used for cloning workflows. They can be used to create genomic libraries or to store specific plasmids that can be used in downstream processes (Inoue et al. 1990). After generating e.g. the desired plasmid via restriction and ligation the amplification was done in DH5α *E. coli* strains for example. Thanks to the exponential growth of these bacteria it is possible to yield relatively high amounts of plasmids.

But first, the plasmids of interests must be internalised by the bacteria and not every bacterium does this willingly. Naturally bacteria can accept new generic information through three mechanism known as transformation, conjugation and transduction (Rahimzadeh et al. 2016). Artificial transformation in the lab is also possible, bur for that bacteria have to be competent. Two different ways to make cells competent for transformation are usually practiced: Heat Shock and electroporation (Chung, Niemela, and Miller 1989; Prakash et al. 2011). We have focused on both in our laboratory.

Electroporation: Neumann and Rosenheck explored that electric impulses lead to temporary permeability changes in biological membranes (1972). These changes allow the passage of DNA (Neumann and Rosenheck 1972) due to reversible pore formation (Sugar and Neumann 1984). This event of pore formation is called electroporation whereas the irreversible process is known as electrofusion happening when two membranes contact (Neumann et al. 1980; Zimmermann et al. 1981). High efficiency transformation of *E. coli* by high voltage electroporation could be observed (Dower et al. 1988)

Chemical competence , and heat shock transformation: The treatment with $CaCl_2$ and following heat shock is the most common way of transformation (Rahimzadeh et al. 2016). The mechanism how the genomic material is internalized via $CaCl_2$ by the cell is not very clear (Rahimzadeh et al. 2016) but there are some suggestions: It is believed that Ca^{2+} is responsible for the interaction between DNA material and the outer lipopolysaccharide (LPS) of the cell membrane (Rahimzadeh et al. 2016). Additionally it is suggested the positive Ca^{2+} ions change the physicochemical behave of lipids and trigger a phase transition of phosphatidylglycerol and LPS (Verkleij et al. 1974; Burnell et al. 1980; Van Die et al. 1983). Ca^{2+} is also given the responsibility for increasing the permeability through structural changes in phosphatidylcholine-cardiolipin bilayers (Gerritsen et al. 1980; Van Die et al. 1983). Rahimzadeh et al. even suggest that the role of Ca^{2+} to increase the membrane permeability is more crucial than the heat shock itself (2016). The understanding of in what

way the transformation proceeds is not enough investigated yet.

We tested two protocols (chapter 3.8.1, 3.8.2) to prepare chemical competent cells and one protocol for the preparation of electrocompetent cells (chapter 3.8.4).

In general transformation experiments can be performed in both gram-positive and gram-negative bacteria (Hanahan 1983). The protocols used in our experiments are based on the Inoue protocol. The protocol by Inoue itself is based on a protocol described by Hanahan (1983), called "Hanahan's method" with a light modification.

1.5.1 The DH5α *E. coli* strain

DH5α cells are bioengineered *E. coli* cells. It has been observed that endonuclease A (endA4+) *E. coli* strains may produce nicked plasmid DNA (Chen and Seeburg 1985; Taylor, et al. 1993). As DH5αs are endA4- they can produce the highest yields of good quality plasmid DNA for double-stranded sequencing (Taylor, et al. 1993). Weng-Tat Chan could find out that Hanahan's method was found to be most effective for DH5α among other strains (Chan et al. 2013).

In this context, our choice using DH5α cells prepared with protocols derived from Inoue protocol is justified.

2 Aim of the thesis

Two major aims were followed in this thesis:

1.: evaluation of fluorescent reporter proteins

Four different fluorescent reporter proteins (mTurquise2, EGFR, dtTomato, iRFP720) were evaluated after transfection into the A549 lung cancer cell line. We evaluated the fluorophores to see if and how they can be analysed by multi-parameter flow cytometry using a (MACSQuant® Analyzer 10, Miltenyi Biotec). In later applications, these fluorophores should act as reporter genes which are coupled to different pathway sensitive promotors.

2. Preparation of competent cells

The aim was to select optimal method for the preparation of competent Bacteria (E. Coli) for the purpose of plasmid production. We have tested one, in in our lab commonly used protocol and a derivation of it, both based on methods using $CaCl_2$.

3 Material and methods

3.1 Technical equipment

Table 2 Technical equipment

Device	Product Number, Supplier, Location
Arium® pro ultrapure water systems	Sartorius®, Göttingen, GER
Biorad PowerPac 200 Electrophoresis Power Supply	4100-101-19, BIO-RAD®, Hercules, CA, USA
ChemiDoc™ XRS+ System	1708265, BIO-RAD®, Hercules, CA, USA
Drying chamber	940557, WTB BINDER®, Tuttlingen, GER
Eppendorf ThermoMixer® C	460-0222, VWR®, Radnor, PA, USA
Gene Pulser XcellTM Electroporation System	165-2660, BIO-RAD®, Hercules, CA, USA
Greiner CELLSTAR® 96 well plates	655160, Sigma-Aldrich®, St. Louis, MO, USA
Heraeus Megafuge 16R Refrigerated Centrifuge 230V	75004270, ThermoFisher Scientific®, Waltham, MA, USA
Herasafe™ KS, Class II Biological Safety Cabinet	51022484, ThermoFisher Scientific®, Waltham, MA, USA
MACSQuant® Analyzer 10	130-105-100, Miltenyi Biotec GmbH, Bergisch Gladbach, Germany
MaxQ Mini 4450 Shaker	SHKA4450-1CE, ThermoFisher Scientific®, Waltham, MA, USA
Microcentrifuge, refrigerated, Micro Star 17R	VWRI521-1647, VWR®, Radnor, PA, USA
MSC -Advantage Class II, Microbiological Safety Cabinet	51025411, ThermoFisher Scientific®, Waltham, MA, USA
Precision balance	Sartorius®, Göttingen, GER
Spectrophotometer, GeneQuant™ 100	SCLI80-2130-00, VWR®, Radnor, PA, USA
Spectrophotometer, NanoVue™ Plus	28-9560-57, VWR®, Radnor, PA, USA
Sub-Cell® GT Horizontal Electrophoresis System	1704401, BIO-RAD®, Hercules, CA, USA
TC-412 Thermal Cycler	FTC41H2D, Techne®, Minneapolis, MN, USA
Ultrasonic Cleaner (waterbath)	470105-414, VWR®, Radnor, PA, USA

3.2 Reagents and media used for bacterial work

Table 3 Reagents and media, bacterial experiments

Media/Reagent	Compounds, Product Number, Supplier, Location
LB-Media (lysogeny broth)	• Bouillon LB, X964.3, Lennox®, Richardson, TX, USA • Agar LB, X965.3, Lennox®, Richardson, TX, USA
Super Optimal Broth with Catabolite (SOC-Media)	• 980ml ddH2O: from arium® pro ultrapure water systems • 5g 0,5% yeast extract: 48503.01, Serva®, Heidelberg, GER • 20g 2% Tryptone: 95039-1KG-F, Sigma-Aldrich®, St. Louis, MO, USA • 10mM Nacl (58,44g/mol): A2942,5000, PanReac Appli-Chem®, Maryland Heights, MO, USA • 2,5mM KCL (74,55g/mol): A2939,1000, PanReac Appli-Chem®, Maryland Heights, MO, USA • 20mM MgSO4 (120,37g/mol): M2643, Sigma-Aldrich®, St. Louis, MO, USA • 20mM Glucose (180,16g/mol): 3,6g in 20 ml of ddH2O, 1.08337.1000, Merck®, Darmstadt, GER
TB-Buffer	for 1L: • 2.38 g 4-(2-hydroxyethyl)-1-piperazineethanesulfonic acid (HEPES); A3724.0500, VWR®, Radnor, PA, USA • 11.2 g CaCl2.H2O • 18.637g KCl • Milli-Q Water • KOH for setting pH to 6,7 • 6.92 g MnCl2

3.3 Media and reagents used for cell culture

Table 4 Media, cell culture

Media	Compounds, Product Number Supplier, Location
DMEM high glucose, 10% FBS, 1% PenStrep	• Dulbecco's Modified Eagle's Medium- high glucose; D5671, Sigma-Aldrich®, St. Louis, MO, USA • 10% Fetal Bovine Serum; F7524, Sigma-Aldrich®, St. Louis, MO, USA • 0.584 g/l L-Glutamine by addition of 200 mM L-Glutamine solution; G7513, Sigma-Aldrich®, St. Louis, MO, USA • 1% Penicillin- Streptomycin (PenStrep); P0781, Sigma- Aldrich®, St. Louis, MO, USA)
RPMI-1640, 10% FBS, 1% PenStrep	• RPMI-1640; R0883, Sigma- Aldrich®, St. Louis, MO, USA • 0.584 g/l L-Glutamine by addition of 200 mM L-Glutamine solution; G7513, Sigma-Aldrich®, St. Louis, MO, USA

Table 5 Reagents, cell culture

Reagent	Product Number, Supplier, Location
Dulbecco's Phosphate Buffered Saline (PBS)	D8537, Sigma-Aldrich®, St. Louis, MO, USA
G-418 solution	G-418 RO, Sigma-Aldrich®, St. Louis, MO, USA
Linear polyethylenimine (LPEI) 10kDa	in- house production at MMCT of University of Vienna by Alexander Taschauer et al.
TrpLE™ Express (1x)	12605-010, Gibco™, Grand Island, NY, USA
Versene™ 1:1500 (1x)	15040-033, Gibco™, Grand Island, NY, USA

3.4 Material for gel electrophoreses

Table 6 Material for gel electrophoresis

Material, Reagent	Compounds, Product Number Supplier, Location
Sodium Borate Buffer (SB-Buffer, 20 x concentrated)	8g NaOH: *A6829,1000, PanReac Appli-Chem®*, Maryland Heights, MO, USA 48g Boric acid: B6768, Sigma-Aldrich®, St. Louis, MO, USA 1000ml ddH2O: from arium® pro ultrapure water systems 6M HCL: hydrochloric acid 30721-M, Sigma-Aldrich®, St. Louis, MO, USA
Agarose SERVA for DNA Electrophoresis	11404.04, Serva®, Heidelberg, GER
2-Log DNA Ladder (0.1-10.0 kb)	N3200L, New England BioLabs®, Ipswich, Massachusetts, USA

3.5 Enzymes

Table 7 Fast digest enzymes, ThermoFisher Scientific, Waltham, MA, USA

Fast Digest Enzyme	Catalogue number	Lot
EcoRI	FD0274	274229
SpeI/BcuI	FD1254	359558
HindIII	FD0504	250958
NdeI	FD0583	203408
PvuII	FD0634	279627

3.6 Plasmids used in transfection experiments

Table 8 Used plasmid reporter constructs with fluorophore genes for transfection experiments

Fluorophore	Reporter Construct	Product number, supplier, location
mTurquoise2	mTurquoise2_NES	Plasmid #36206, Addgene, Cambridge, USA
eGFP	pMuLE_ENTR_C MV_eGFP_R4-R3	Plasmid #62141, Addgene, Cambridge, USA
tdTomato	pMuLE ENTR CMV tdTomato R4-R3	Plasmid #62151, Addgene, Cambridge, USA
iRFP	pMuLE ENTR CMV iRFP R4-R3	Plasmid #62158, Addgene, Cambridge, USA
3P-Top	pMuLE_EXPR_C MV-eGFP_TOP-iRFP_hPTCH1-mTur-quoise2_CBF-tdtomato	Cloned by Julia Maier in the MMCT lab by ligation reactions, recombination and cloning into One Shot TOP10

3.7 Experiments with bacteria

3.7.1 Preparation of chemical competent cells, method A

First, TB buffer was prepared as follows: in 1L Milli-Q Water 2.38 g HEPES (final concentration 10 mM), 11.2 g CaCl2.H2O (final conc. 75 mM) and 18.637g KCl (final conc. 250 mM) were solubilized. The pH was adjusted to 6.7 with KOH, and then 6.92 g MnCl2 (final conc. 55mM) was added. Finally, the buffer was sterilized with a 0.22 μm filter.

Of DH5α *E. coli* , a colony was picked from a already cultured LB plate, or fresh bacteria were scraped from a glycerol stock. In the next step, these bacteria were cultured in a pre-culture, at room temperature overnight in 62.5 mL LB in a 250 mL Erlenmeyer flask, shaking at 180 rpm. For later use, 250 mL SOC or LB medium was warmed up at 23°C.

The next morning was dedicated to rearing a bacteria culture of an exact OD_{600} (optical density at 600 nm): In a first measurement, pure LB medium was used as blank value. Afterwards 250 mL of pure LB medium was inoculated with 3 ml of the overnight DH5α pre-culture, in a 1 L flask. Its OD_{600} was also measured as t_0. The culture was incubated at 37°C and 180 rpm under observation of the bacterial growth via OD_{600} measurement. After

approximately 1,5 hours and 15 measurements an OD_{600} of 0.4 – 0.45 (Figure 20, method A) was reached which was considered as optimal.

After reaching the desired density, the culture was immediately chilled for 10 minutes in a 4°C ice slush. From that step, onwards the bacteria needed to remain at 4°C. Bacs were aliquoted in 5 pre-cooled CT50 tubes and centrifuged at 2500 x g at 4°C for 10 minutes. Acceleration was set to 9 and deceleration to 7. Supernatant was discarded and the pellets were resuspended in 1 mL ice-cold TB-buffer. Every resuspended aliquot was then pooled in one CT50 tube so that it was filled with 25 mL in total. Then the bacs were centrifuged under the same conditions as above again. The supernatant was discarded and the pellet resuspended in 1 mL of TB-buffer and then filled up with the TB-buffer to 20 mL. Then 1.5 mL RT (room temperature) DMSO was added and mixed by turning the CT50 tube twice. After an incubation time of 10 minutes, the suspension of the bacteria was quickly aliquoted into epis (~ 200μL per epi), put on dry ice, and transported into the -80°C freezer.

3.7.2 Preparation of chemical competent cells, method B

Picked bacteria were cultured at 37°C overnight in 5-25 mL LB in a 5-25 mL Erlenmeyer flask at 180 rpm. For later use, 250 mL SOC or LB media was warmed up to 23°C.

The next morning two OD600 (optical density at 600 nm) measurements had been done. First an OD measurement of the pure LB media. This was our blank. Afterwards 250 mL of this media was inoculated with 3 ml of the overnight DH5α culture in a 1 L flask. Its OD_{600} was also measured as t_0. The culture was incubated at 37°C and 180 rpm under observation of the bacterial growth via OD_{600} measurement. An OD_{600} of 0.4 – 0.45 was considered as optimal and have been reached after 1.5 hours and 5 measurements (Figure 20, method B).

After reaching the desired density the culture was immediately chilled for 10 minutes in a 4°C ice slush. From that step on it was crucial always keeping the bacs on 4°C. Bacs were aliquoted in 5 pre-cooled CT50 tubes and centrifuged at 3500 x g at 4°C for 10 minutes. Acceleration was set on 9 and deceleration on 7. Supernatant was discarded and the pellets were resuspended in 1 mL ice-cold TB-buffer. Every resuspended aliquot was then pooled in one CT50 tube so that it was filled with 50 mL in total. After incubation time of 10

minutes the bacs were centrifuged under the same conditions as above again. The supernatant was discarded and the pellet resuspended in 18,6 mL of TB-buffer and then 1.4 mL room – tempered DMSO was added and mixed well by turning the CT50 tube twice. After an incubation time of 5 minutes the suspension of the bacteria were quickly aliquoted into Epis put on dry ice and transported into the -80°C freezer.

3.7.3 Heat Shock Transformation

Heat shock transformation was performed in chemical competent *E. coli* DH5α cells (or Stbl3). It is suggested that by stressing bacteria with quickly increasing temperature eases DNA entry as it is explained that the heat increase causes reduction in membrane potential by which the intracellular milieu get less negative and consequently the negatively loaded DNA enters the cystol easier (Panja et al. 2006). Chemical competent DH5α were taken out from the -80°C freezer and thawed in 4°C ice slush. Thawing on ice is crucial due the bacteria's sensitivity to high temperature. Protein activity is involved in this heat sensitivity (Chang et al. 2013). As temperature increases the protein activity decreases and so does the performance of the cell. Consequently fast working is recommended. 50μL of DH5α was combined with plasmid DNA (1 to 2 μL at least) in pre-cooled Epis. As a negative control, μL of bacteria received no plasmid. After pipetting, the bacteria were put on ice for 30 minutes, then heat shocked in a water bath at 42°C for 45 seconds, then incubated on ice again for 2 minutes. For the outgrowth phase, 450 μL of SOC was added per epi. After a further incubation time of 45 minutes at 700 rpm and 37°C, the bacteria were streaked on the respective labelled and pre-heated LB, plates and incubated overnight at 37°C. Observation of the plates was done the next morning. For downstream processes, the plates could be directly used or stored at 4°C.

3.7.4 Preparation of electrocompetent Cells

The first step in this protocol is again the generation of a bacteria culture of a specific OD600, similar to above. For this, DH5α *E. coli* were streaked out on LB agar, and incubated overnight at 37°C. The next day, 5mL of LB medium were inoculated with a single colony in a sterile 50 mL falcon, tube and incubated overnight at 37°C and 200 rpm. The next day, 0.5 mL of this culture was added to 40 mL LB media in a 150 mL Erlenmeyer.

Bacteria were incubated at 37°C in a waterbath for 1.5 hours until an OD_{600} of 0.4 was reached. The flask was then put on ice slush, and shaken gently to cool the cells as fast as possible. From now, on the cells were always kept on 4°C. The bacteria were transferred into a pre-cooled 50 mL falcon tube and centrifuged for 7 minutes at 4600 x g at 4°C. After centrifugation, the supernatant was aseptically poured off, and the cell pellet was suspended in 4 °C ice-cold ddH_2O. Afterwards, 30 mL of ddH_2O was added, and then mixed by inverting the tube several times. In the following step, the suspension was centrifuged again under the same conditions as before. After discarding the supernatant, the pellet was gently resuspended in 1 mL ice-cold ddH_2O again, transferred into pre-cooled epis and centrifuged for 30 to 60 seconds at 10.000 x g at 4°C. The supernatant was carefully removed and the pellet resuspended in 1 mL ice-cold ddH_2O and then centrifuged as before. After that, the supernatant was discarded and the pellet suspended in 200 – 800 µL ice-cold ddH_2O. At this point the cells can directly be used for electroporation, or frozen at -80°C.

3.7.5 Electroporation

Firstly, the electroporator (Gene Pulser Xcell^{TM} Electroporation System, Bio-Rad) was turned on and set to 1.7 – 2.5 kV, 200 Ohms and 25 µF. A recovery SOC medium was placed in a 37°C waterbath or incubator. Freshly made electrocompetent DH5α cells were used, or frozen cells that were thawed on ice. Appropriate number of epis and 1 mm electroporation cuvettes (Gene Pulser$^{®}$/Micropulser™ 0,1 cm electroporation cuvettes) were placed on ice. The cuvettes have been placed in bags, to protect from humidity, when cooling them subsequently at 4°C. The tube which contained the cells was flicked a few times to mix, and 25 µl of the cells were added to the cooled empty epis. 1µl of the DNA solution of interest (considering its concentration) was then added to the cells. Afterwards the DNA/cell mix was transferred to the cold cuvette and taped on the workspace two times to make sure the mix was on the bottom and not on the side areas of the cuvette's capillary. Next, it had to be made sure that the exterior of the cuvette is dry. The dry cuvette was put into the electroporation device and "pulse" was pressed once. Immediately, the bacteria were pipetted into 975 µl of 37°C SOC and mixed by pipetting up and down. For recovery, the bacs were put in a rotating incubator for one hour.

3.7.6 Plate Streaking of transformed bacs

After finishing the transformation process, the bacs were diluted in SOC media 1:10, 1:100 and 1:1000. LB – plates were used for streaking. For the survival control, a plate without an antibiotic was used for streaking. The pure bacteria suspension and the dilutions were streaked on three plates each with an antibiotic. Which antibiotic depended on the resistance gene of the used DNA. The streaked plates were incubated overnight at 37°C.

3.7.7 Determining transformation efficiency

For determining the quality of the bacs, the transformation efficiency was tested. It is tested with the transformation of the pUC19 plasmid because its high performance being copied. For testing the efficiency of the chemical competent cells, four LB + AMP plates and one LB plate (as a positive control) were used. The plasmid was diluted to 100 pg/µL. The transformation was done via heatshock as described in 3.7.3. The transformations were diluted 1:100. 30 µl of each dilution was plated on the prepared plates. After an overnight incubation, the colonies on every plate were counted. Then, the meancolony number for all four replicate plates were determined, and the transformation efficiency calculated as follows:

$$\frac{Mean\ number\ of\ colonies}{\mu g\ of\ plasmid\ DNA\ used\ x\ Dilution}$$

The efficiency of the transformation via electroporation was determined as follows: As three electroporation-transformation dilutions were streaked on plates the efficiency of each dilution was calculated.

$$\frac{\dfrac{Colonies\ counted\ on\ all\ three\ plates}{3}}{\mu g\ of\ plasmid\ DNA\ used\ x\ fraction\ used}\ x\ Dilution\ factor$$

3.8 Cell culture

3.8.1 Cell maintenance of A549

A549 cells were used for the transfection experiments (CRM-CCL-185TM, ATCC®, Manassas, VA, USA). The cells were kept in a 75 cm^3 cell culture flask in an incubator at 37°C and 5% CO_2 which is defined as standard conditions. They grew in fully formulated RPMI (10 % FBS, 1% PenStrep, 1% Glutamine). Cells were splitted 1:12 within three to four days to avoid overgrowth and following death. The cells' condition was checked by microscopy. To split, the medium was aspirated. Next, the attached cells were washed with 5 mL of PBS. To detach the cells from the bottom of the flask, 3 mL of TrypLe^{TM} (12605-010, Gibco™, Grand Island, NY, USA) was added, and then incubated for 5 minutes in the incubator under standard conditions. To detach as many cells as possible, it was important to tap on the bottom and the sides of the flask. While tapping, a horizontal movement was suggested. To get sure that a maximum number of cells was detached, a look into the microscope is recommended. Then the cells were suspended in basal RPMI and transferred into a centrifuge tube and spun down at 200 x g for 5 minutes. Meanwhile, a new flask with fully formulated RPMI was prepared and placed into the incubator. After centrifugation, the supernatant was discarded and the cells resuspended in 1 mL of fully formulated RPMI. An aliquot was taken and put in the already prepared flask and incubated at 37°C.

3.8.2 Transfection of A549s

The process of transfection took three days. Transfections were performed in 96 – well plates (F-bottom, CELLSTAR® from greiner bio-one, Cat.-No. 655 160). The plasmid DNA (pDNA), in this case, fluorophore reporter constructs, of interest firstly have been thawn on ice and kept at 4°C). Cells should be transfected with 200 ng of pDNA per well. Into each well 10.000 cells were seeded. This cell amount was gained by counting the cells in a Neubauer Chamber. Therefore, the cell splitting protocol as described in 3.8.1 was followed till the cell pellet was gained. This pellet has been resuspended after the centrifugation step. From this suspension, a 1:20 dilution was prepared. Fully formulated medium was used as diluent. Cell counting was made with the Neubauer Chamber. After determining the number of cells in the dilution the amount needed to get 10.000 cells in each needed well was known. Every well was then filled up to 200 µL with fully formulated medium.

The wells at the edges were filled with PBS to keep cells in a humid environment. For better handling, for one more well for each condition was calculated. The well plate was put into the incubator at the next step. In the meanwhile, the polyplex solutions were prepared:

Experiments were done in quintuplicates (used five wells) and we calculated for six wells. Volumes of DNA and LPEI solutions to polyplex had to be the same. To get the same volume, LPEI and pDNA were diluted with HBS buffer (20mM HEPES, 150 mM NaCl, pH 7,1). Table 9 demonstrates an example for a polyplex solution calculation in detail. 200 ng of pDNA was used for each well and calculation were done for six wells although 5 wells were needed. 200 ng of pDNA was needed per well. Finally, the LPEI solution was put to the pDNA solution and mixed by flash pipetting. Flash pipetting is a method to mix solutions by pipetting up and down in a fast way for approximate thirty times. After adding the polyplex solutions into the respective wells, the plate have been incubted for 4 hours at 37°C. Then 100 μL of prewarmed complete medium have been added in each well and incubated overnight at 37°C.

Table 9 Calculations of polyplex solutions of mT2 and eGFP reporter plasmids in detail. The volumes of LPEI and pDNA solutions are the same. Both solutions were prepared by dilution in HBS. Finally, the LPEI solution was put to the pDNA solution and mixed by flash pipetting. That should ensure a as possible homogenous mixture. The polyplex solution was immediately added to the cells after preparing it.

Polyplexing mT2			**Polyplexing eGFP**		
Substances:			**Substances:**		
pDNA (conc.; µg/ml)	630,8		pDNA (conc.; µg/ml)	284	
LPEI (conc.; µg/ml)	157,5		LPEI (conc.; µg/ml)	157,5	
pDNA/well (µg)	0,2		pDNA/well (µg)	0,2	
number of wells	6		number of wells	6	
pDNA (total amount; µg)	1,2		pDNA (total amount; µg)	1,2	
LPEI (calculation)			**LPEI (calculation)**		
N/P ratio	9		N/P ratio	9	
LPEI amount nee-ded (µg)	1,41		LPEI amount nee-ded (µg)	1,41	
volumes needed			volumes needed		
total volume (µl)	60		total volume (µl)	60	
	LPEI stock (µl)	**HBS stock (µl)**		**LPEI stock (µl)**	**HBS stock (µl)**
LPEI	8,94	21,07	LPEI	8,94	21,17
	pDNA stock (µl)	**HBS stock (µl)**		**pDNA stock (µl)**	**HBS stock (ul)**
pDNA	1,90	28,1	pDNA	4,23	25,78

3.8.3 Evaluation of transfection experiments

All transfection experiments were evaluated by flow cytometry (MACS QUANT® 18 Analyzer 10, MACS Miltenyi Biotec). After finishing transfection as described in 3.8.2 the media was aspirated from each well. Then the wells were filled up to 200 µL with PBS to wash. PBS was aspirated from each well. To detach cells from the surface 20µL of Tryp-sin was added in each well and incubated fort five minutes at 37°C. Then the wells were filled up to 200µL PBS. Before the volume was taken up from each well, the suspension had to be mixed before to get a homogenous cell suspension for measuring. To avoid bub-bles the cell suspension was mixed manually with a pipette instead with the integrated

pipette on the flow cytometer. Untreated cells were used as negative control to exclude autofluorescence. Cells passing through the excitation laser light are scattering it. This light scatter ist detected as FSC (=Forward Scatter, correlates with cell size) and SSC (=Side Scatter, correlates the granularity of the cell). In this manner, our cell populations could be distinguished based on their size and as result measurements with single cells colonies were possible. Light emission of single cells shine through emission filters (explained below) set on 483 – 493 nm.

Every cell was excited with a laser with the appropriate wavelength. The light emission of the fluorescent reporter proteins was then catched by emission filters. These filters allow measurements of emission with a certain wavelength spectrum that is within the general emission spectrum of the fluorophore. The emission of one fluorescent reporter protein was first measured through its appropriate filter then through filter of the other fluorophores. The following table (Table 10) shows in detail the excitation wavelength, filters used in our measurement and our tested proteins.

Table 10 Overview of the different MACSQuant instrumental configurations used in our experiments.

Excitation Laser	Channel	Emission Filter *	Tested fluorescent reporter proteins
Violet 405 nm	V1	450/50 nm	mTurquoise2
	V2	525/50 nm	
Blue 488 nm	B1	525/50 nm	EGFP
	B2	585/40 nm	
Red 635 nm	B2	585/40 nm	IRFP
	B3	655-730 nm	
Red 635 nm	R1	655-730 nm	tdTomato
	R2	750 nm LP **	

* interpretation of wavelength spectrum of the MACSQuant emiossion filter: e.g. V1: 450/50 nm means that the wavelength spectrum measured is between 425 and (+50) 475 nm, for B1: 525/50 nm means that the wave length spectrum measured is between 500 and (+50) 550 nm and so on.
** LP = Long pass filter: allow transmission of photons above a specified wavelength

The measured data was saved as "*.mqd" and "*.fcs" files. For further analysis, the "*.mqd" files were used. Analysis was performed in FlowJo X (www.flowjo.com, Ashland, Oregon, USA). Figure 13 shows the gating strategy used in untreated cells and of mTurquoise2 transfected cells. This strategy was used in each transfection experiment.
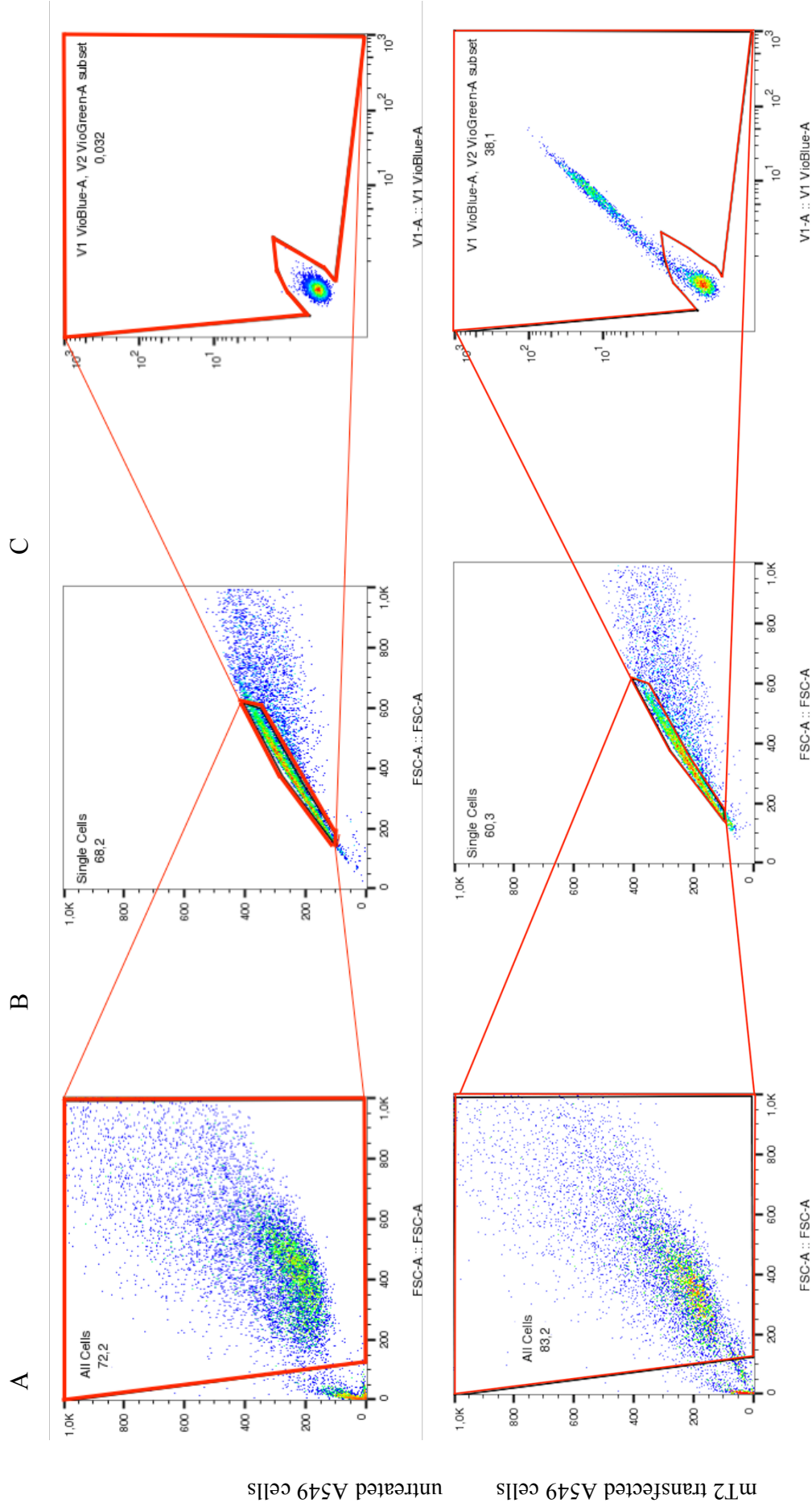
Figure 13 Gating strategy showed on untreated (first row left to right) and mT2 transfected (second row left to right) A549 cells. A | Signal of all cells detected by the flow cytometer. In A, the cell debris at the bottom left were excluded. **B** | Gating of single cells: >60% of all cells are single cells. **C** | untreated cells: Every cell has an autofluorescence in each channel. This self fluorescence had to be excluded to get realistic results. Therefore, untreated cell were also measured in each channel. We considered autofluorescence signal of < 0,1% in the used channel as optimal. This figure shows that 0,032% of untreated cells and 38,1% of mT2 transfected cells showed a signal in the mT2 channel.

3.9 Fluorophore genes

3.9.1 Preparation of the reporter construct

All original plasmid constructs were obtained via Addgene, Cambridge, USA in DH5α *E. coli* strains. The bacteria, contained pMule_ENTR_CMV-iRFP_R4-R3 and pMule_ENTR_CMV-tdTomato_R4-R3 were streaked on a LB plate with Kanamycin (Kanamycin sulfate from *Streptomyces kanamyceticus*, Cas-Number: 25389-94-0; Sigma-Aldrich®, St. Louis, MO, USA) as antibiotic, and cultivated overnight at 37°C. At the next morning, single colonies of the overnight were picked and pre-cultured in a CT50 filled with 5 -10 mL of LB media, also treated with Kanamycin for selective growth. At evening, approximately 7 hours later 25µL of the pre-cultured bacs were cultured overnight at 200 rpm and 37°C in a 1 L flask with 250 mL LB media treated with 4µL of antibiotic per mL. ThermoFischer suggests that generally a 250 mL of overnight bacterial culture grown in LB medium is sufficient for good yield of plasmid DNA. But it is important not to exceed recommended cell mass, what is culture volume $\times$ OD$_{600}$, because it may decrease quality of isolated DNA ('GeneJET Plasmid Maxiprep Kit User Guide - Thermo Fisher Scientific'). The maximum culture volume to use can be determined using formula below:

$$Maximum\ Culture\ Volume\ (mL) = \frac{750}{OD_{600}}$$

('GeneJET Plasmid Maxiprep Kit User Guide - Thermo Fisher Scientific'). After determining the volume to use isolation of the pDNA was processed with the "GeneJET Plasmid Maxiprep Kit". After successful isolation, the concentration of the DNA has been measured via Spectrophotometry, (NanoVue™ Plus). The identity of the isolated plasmid was afterwards tested via diagnostic restriction digest (DRD) (3.9.2).

3.9.2   Diagnostic Restriction Digest (DRD): its planning and analytics

Performing of DRDs are necessary to analyse if right DNA had been isolated out of the bacteria. In the very first step a plasmid map was generated with the SnapGene Software (GSL Biotech LLC5211S, Kenwood Ave, Chicago). This software, among other features helps its user to decide which restriction enzymes could be used for restriction digest planning by offering a simulation of the resulting bands. It also shows a plasmid map to get a practical overview of its characteristics.
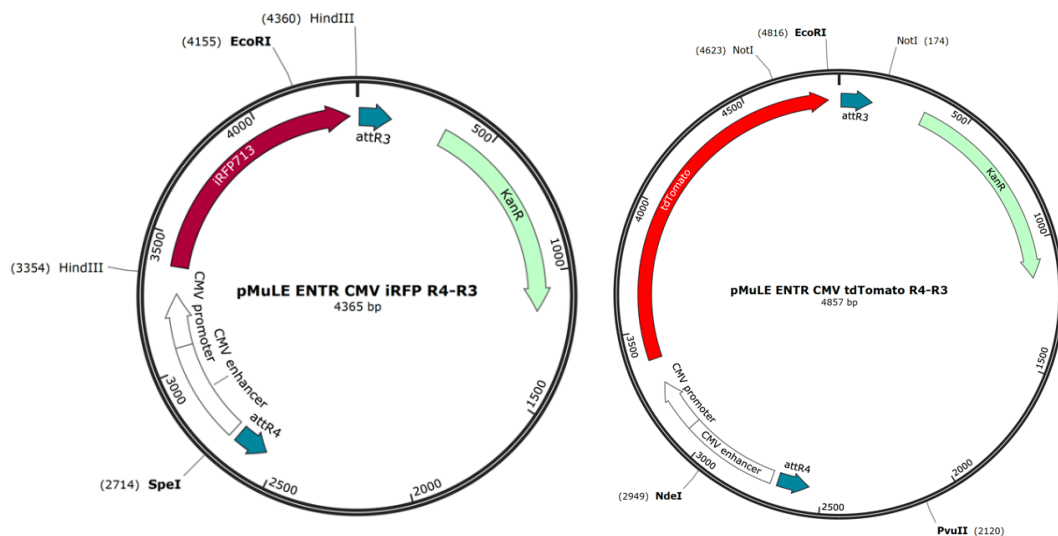
Figure 14 Plasmid map of pMule_ENTR_CMV-iRFP_R4-R3 (left) and pMule_ENTR_CMV-tdTomato_R4-R3 (right). The plasmids and some of its characteristics are demonstrated in this image. EcoRI, HindIII and SpeI were used for the plasmid left whereas, EcoRI, NdeI, NotI and PvuII are the restrictions enzymes used in DRD of the plasmid on the right. The restriction site of each enzyme is also shown in brackets. Both contain the genes coding for Kanamycin resistance for selective growth in bacteria. Both plasmids have been constructed witch SnapGene software.

PMule_ENTR_CMV-tdTomato_R4-R3 and pMule_ENTR_CMV-iRFP_R4-R3 are shown as an example in Figure 14. At least 200 ng of each plasmid were pipetted together with 1 µL of the restriction enzymes and 2 µL of the Fast Digest Green Buffer (10x) in one PCR epi and then diluted up to 20 µL with nuclease free water. The restriction enzymes for each plasmid and their restriction sites are shown in Figure 14. For the digestion step itself the epis were put into the Thermal Cycler TC-412. Digestion program: 120 minutes at 37°C, 10 minutes 80°C. After digestion, the samples were stored at 4°C or directly used for downstream processe. The analysis of DRD after gel electrophoreses was done by an

agarose gel. Afterwards, the gel was analysed using the ChemiDoc™ XRS+ System Imager. The band pattern in the gel was then compared with the previously simulated pattern from SnapGene (see 4.2, Figure 18).

4 Results

4.1 Transfection of A549 with N/P 9 is more efficient than N/P 6

As the usage of more LPEI leads to increased cell toxicity we at first tried out two different N/P ratios to finally decide which one is more ideal for our experiments. Therefore, the first experiment was performed with a ratio of N/P 6 and N/P 9. 10.000 cells were seeded in each well (see 3.8.2) and transfected with mTurquoise2. We have chosen mT2 for this experiment because a colleague in our laboratory had already done satisfying experiments with it.

Our results have shown significant increase of positive transfected single cells when N/P ratio of 9 was used in comparison to N/P ratio of 6. When used N/P 9 38,1% of the single cells showed positive events while N/P 6 condition showed 33,1% positive events (Figure 15). The amount of positively transfected cells was measured by the emission of mt2 in the V1 and V2 channel. Figure 16 shows the gating of A549 cells used in the N/P decision experiment
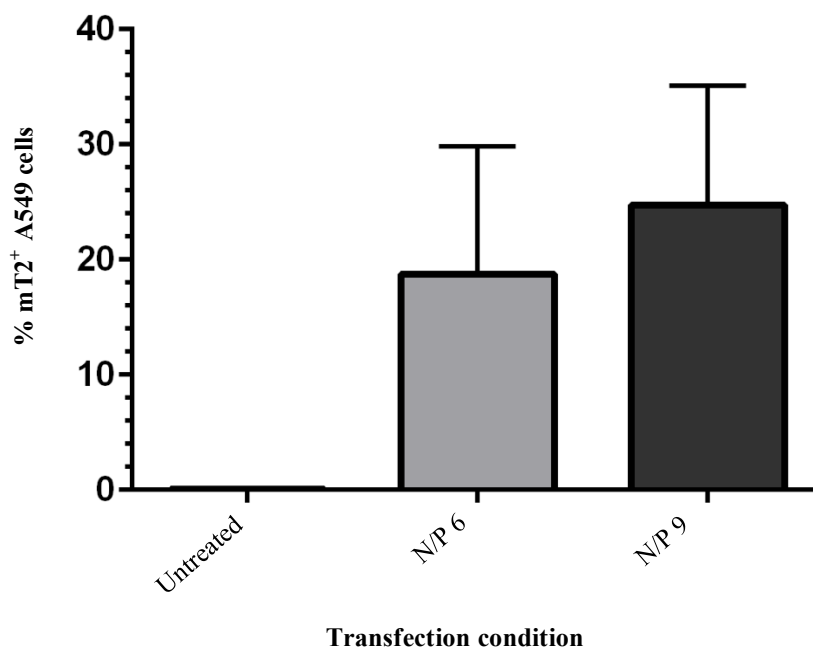
Figure 15 Events of mT2^{+} A549 cells measured via flow cytometry. This experiment have shown that more positive transfection events could be obtained when A549 cells are transfected with N/P 9.
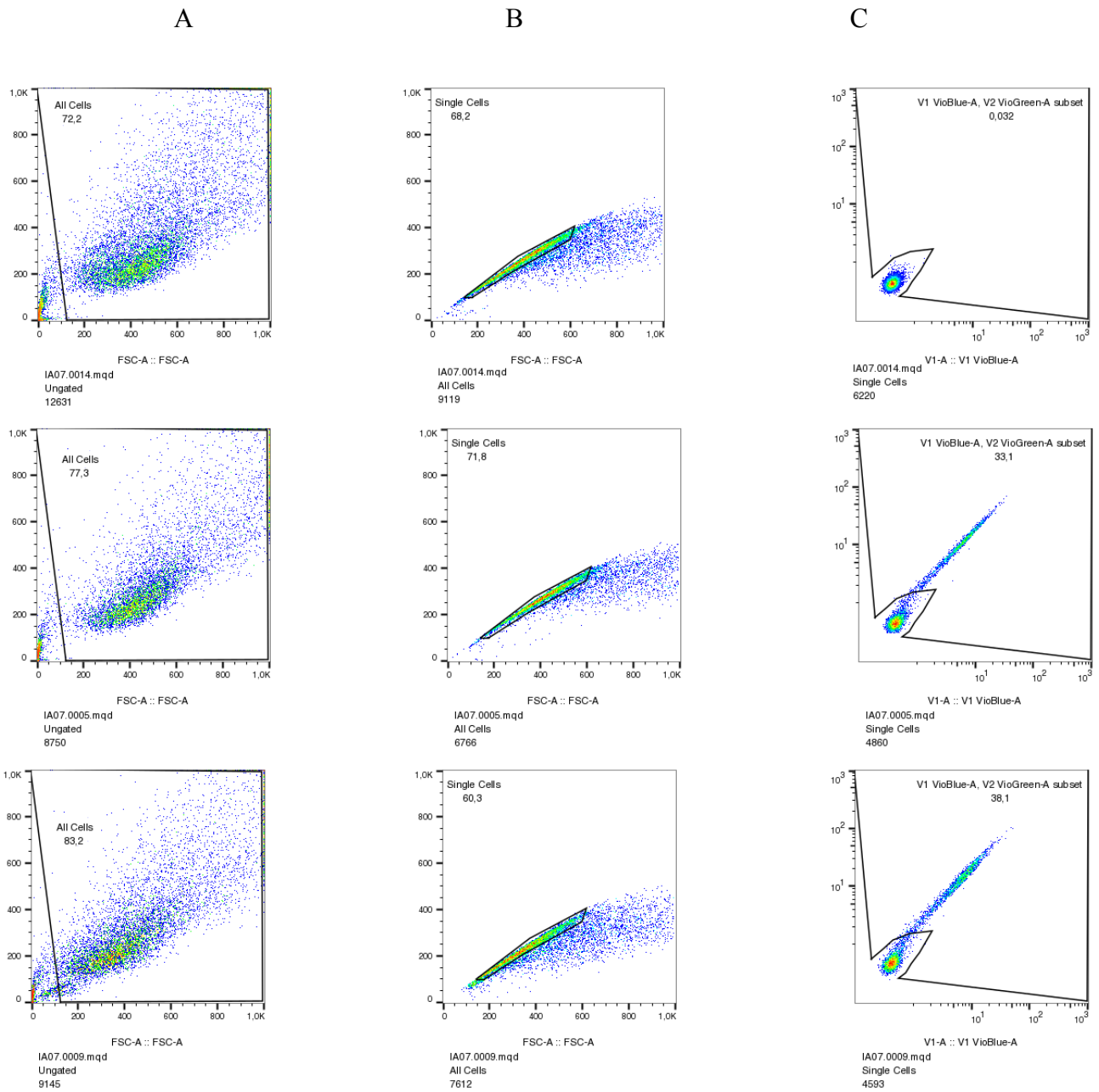
Figure 16 Gating of A549 cells used in the N/P decision experiment. A | Gating of untreated cells with 0,03% events in the mT2 channel. **B |** Gating of mT2$^+$ cells transfected with N/P ratio of 6 showed 33,1% positive events. **C |** Gating of mT2$^+$ cells transfected with N/P ratio of 9 showed 38,1% positive events.

4.2 Preparation of the reporter constructs and following gel electrophoreses

Reporter constructs for iRFP and tdTomato had to be prepared as described in 3.9. The gel pattern after the DRD showed bands as simulated. Figure 17 shows our resulted gel pattern and figure 18 represents a comparison of both, the computed and the resulted gel. As the both show similarity the preparation of the right plasmids is approved.
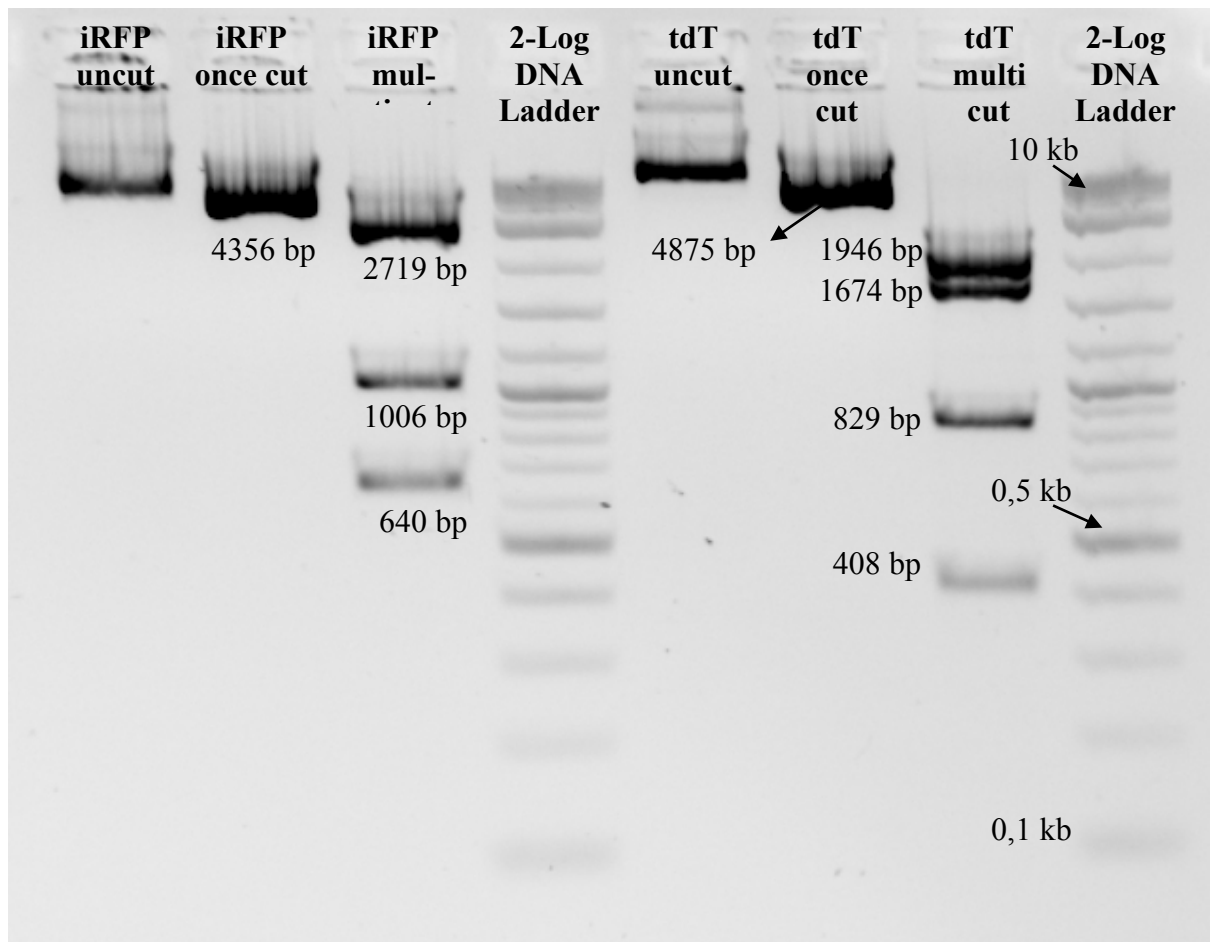
Figure 17 Pattern of digested fluorophore reporter constructs | DRD (see 3.8.2). Pattern was similar with the excepted one (see comparison, Figure 12) | Gel conditions: 1% agarose gel, Ethidium Bromide as stain to visualize bands, running time: 1hour at 80V, ladder: 2 - log DNA ladder (0,1 – 10 kb; full annotation see Figure 18)
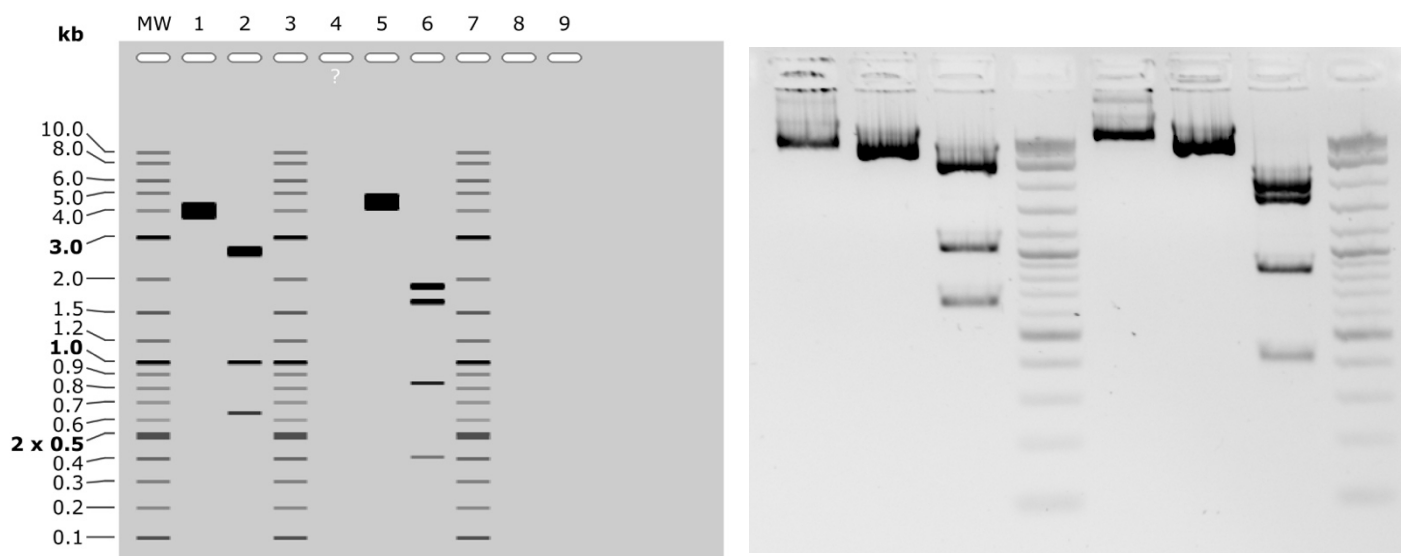
MW: 2-Log DNA Ladder

1: pMuLE ENTR CMV iRFP R4-R3
   EcoRI
   1. 4365 bp

2: pMuLE ENTR CMV iRFP R4-R3
   HindIII + SpeI
   1. 2719 bp
   2. 1006 bp
   3. 640 bp

3: 2-Log DNA Ladder

4: pMuLE ENTR CMV tdTomato R4-R3

5: pMuLE ENTR CMV tdTomato R4-R3
   EcoRI
   1. 4857 bp

6: pMuLE ENTR CMV tdTomato R4-R3
   NdeI + NotI + PvuII
   1. 1946 bp
   2. 1674 bp
   3. 829 bp
   4. 408 bp

7: 2-Log DNA Ladder

Figure 18 Comparison of computed gel pattern (left image) and resulted gel image of the DRD of pMule_ENTR_CMV-iRFP_R4-R3 and pMule_ENTR_CMV-tdTomato_R4-R3. The computed image has been created with SnapGene software and so provided us a prediction of the expected gel pattern. The direct comparison of both suggests that the right plasmids has been prepared.

4.3 Chosen fluorophores have shown interferences

First the cells have been transfected with a single fluorophore. Each fluorophore's light emission characteristics have been observed in its own channel and afterwards in the channels of the other fluorophores. Also, transfection-duos and multi-transfections have been tested in the same way. Investigating how and if fluorophores shine in other fluorophore channels is crucial for associated downstream experiments. In our results, we could observe emission interferences. The result of each condition is described in the following Table 11 summarises the results. Figure 19 shows the gating strategy used on mt2 transfected A549 cells.
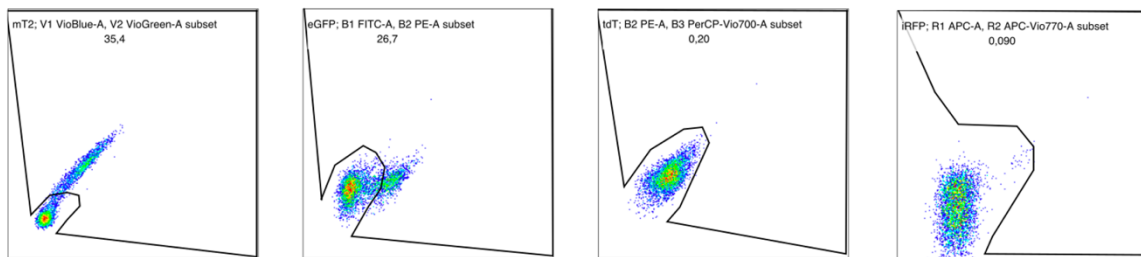
Figure 19 An example of results of the gating demonstrated on mT2+ cells (same strategy was used on every condition. This figure shows how mt2+ shines in the channels of the other investigated fluorophores.

Table 11 Amount of all fluorophore-positive cells captured in the mt2 (V1:V2), eGFP (B1:B2), tdTomato (B2:B3) and iRFP (R1:R2) channel

Transfection condition			% of transfected cells shining in tested channels			
			mT2 V1:V2	eGFP B1:B2	tdT B2:B3	iRFP R1:R2
	Single transfections	mt2	35,4	26,7	0,2	0,1
		eGFP	10,2	52,7	38,8	0,2
		tdT	0,4	38,5	31,8	0,5
		iRFP	0,00	0,1	0,2	9,7
	Co-transfections (Duos)	mT2/eGFP	38,7	46,1	20,9	0,1
		mT2/tdT	24,0	24,1	24,2	0,1
		mT2/iRFP	27,2	17,0	0,2	2,3
		eGFP/tdT	5,0	43,5	38,0	0,2
		eGFP/iRFP	3,0	50,5	30,6	10,1
		iRFP/tdT	28,8	19,8	10,2	1,0
	Co-transfectios (multi Flourophores)	mT2/eGFP/tdT/iRFP	17,6	40,4	29,1	4,4
		3P-TOP	7,0	15,1	11,5	0,1

Results of single fluorophore transfections (Figure 20)
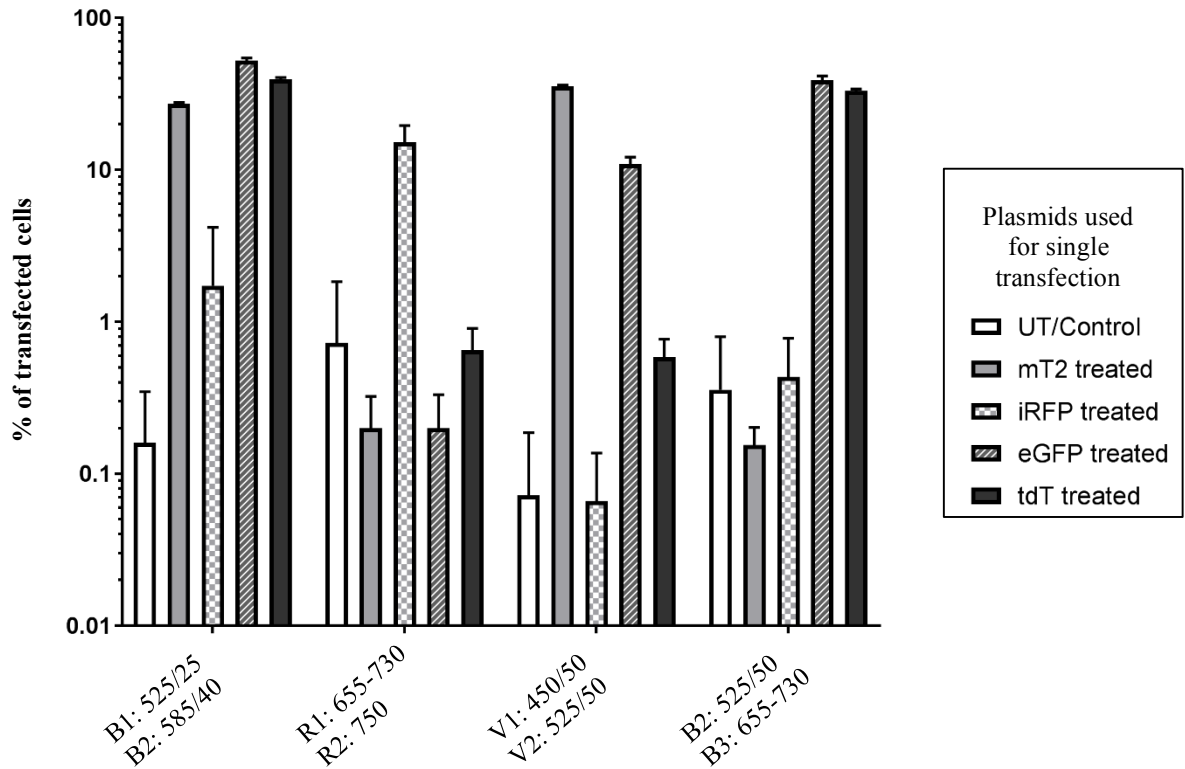
Emission filter spectra by Miltenyi MACSQuant® Analyzer 10 in nm

Figure 20 Emission signal of solo transfections. A549 cells have been transfected with respectively one fluorophore reporter plasmid that are shown in the legend box of this figure. The amount of positively transfected cells is the average of 4 measurements. mT2 transfected cells: 35,40% of cells gave a signal in the mT2 channel and 26,70% in the eGFP channel. Apparently mT2 transfected cells showed interference with eGFP excitation spectrum. Looking at eGFP transfected cells 52,70 % percent of the cells gave a positive signal in the eGFP channel and 38,80 % in the tdT which is a clear interference. 10,20 % of these cells also showed a signal in the mT2 channel. 38,50 % of the tdT transfected cells showed action in the eGFP channel and 31,80 % in tdT channel. The amounts shined in mT2 and iRFP channels were less than 1%. Only 9,69 % of iRFP transfected gave an iRFP

Co – transfection: Fluorophore – doublets (Figure 12)
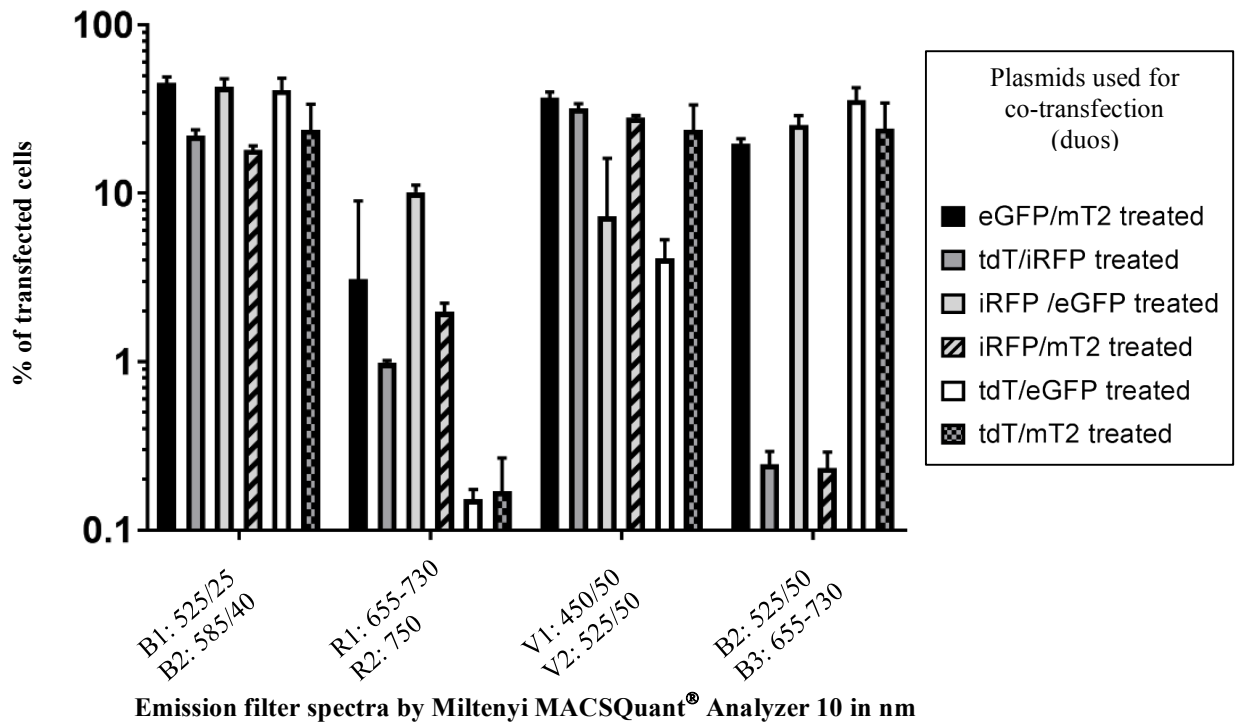
Figure 21 Emission signal of cells transfected with two plasmids. A549 cells have been transfected with respectively two fluorophore reporter plasmids. The combinations are shown in the legend box of this figure. The amount of positively transfected cells is the average of 4 measurements.

In this condition cells were transfected with two fluorophore reporter plasmids to observe if their emission spectra overlap. (Figure 21)

mT2+eGFP transfected cells:

46,10 % percent of transfected cells showed a signal in the EGFP channel. A signal occurred in the iRFP which can be disregarded as it was very little. 38,7 % of the cells showed signal in the mT2 channel and approximately 20% in the tdTomato channel.

mT2+tdT transfected cells:

Approximately a quarter of the cells showed signal in the mT2 channel and another quarter in the EGFP channel. ~ 23% showed signal in the EGFP channel.

mT2+iRFP transfected cells

Only 2,32 % of cells showed signal in iRFP channel, 27,20 % in the mT2 channel and 17,00 % in the EGFP channel

eGFP+iRFP transfected cells:

41,5 % of transfected cells showed signal in the EGFP channel but only 8,95% in the iRFP channel. 22% showed signal in the tdT channel and 6% in the mT2 channel.

eGFP+tdT transfected cells:

Nearly half of the cells were EGFP positive, 43,50 % were positive in the in the tdT channel and 4,95 % in the mT2 channel and less than 0,20 % signal occurred in the iRFP channel.

tdT+iRFP transfected cells:

This condition showed a low signal in the iRFP (1,02 %) and tdT (10,20 %) channel, but much more events in the eGFP (19,80%) and mT2 (28,80%) channels.

Co – transfection:
All four Fluorophores together and 3P-TOP as single transfection (Figure 22)

Cells transfected with all four fluorophore reporter constructs gave a signal in every channel observed. Equally 3P-TOP transfected cells did. To emphasize it again, 3P-TOP is a reporter construct containing the genetic information for every used fluorophore. Remarkably, the amount of iRFP$^+$ cells are very low (Figure 22).

Emission filter spectra by Miltenyi MACSQuant® Analyzer 10 in nm
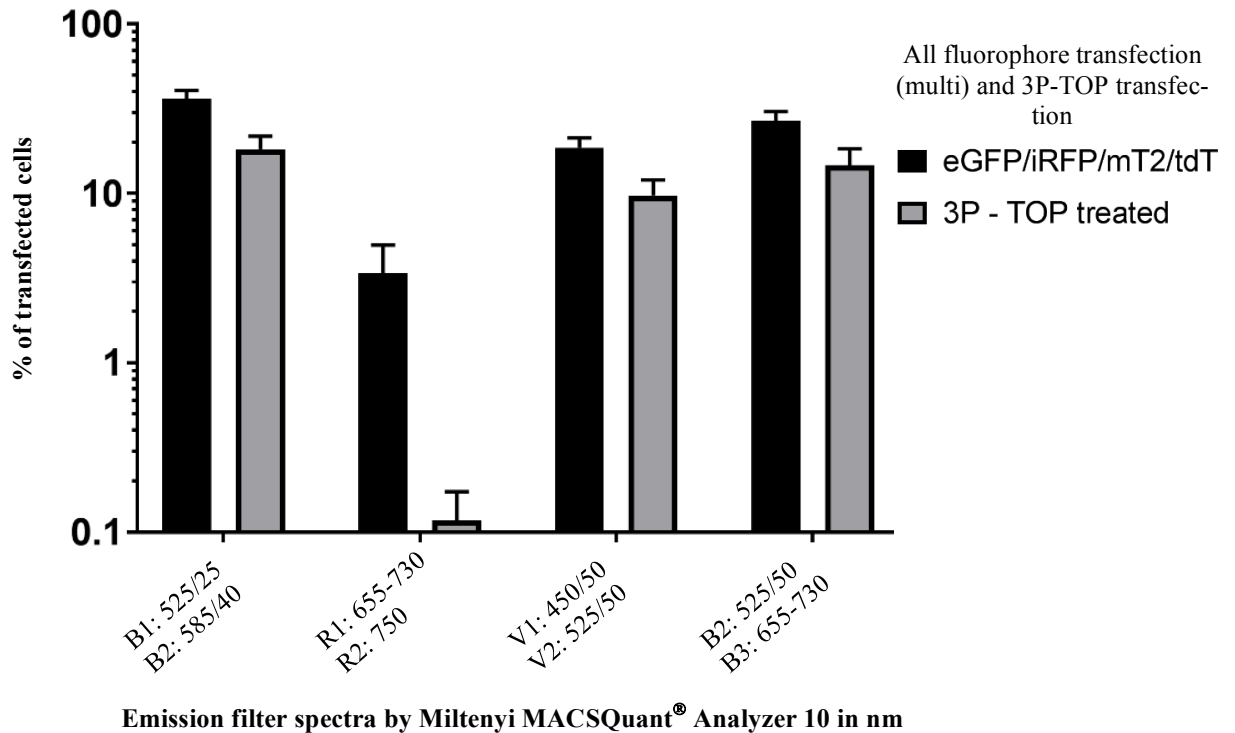
Figure 22 Cells transfected with all four fluorophores reporter constructs and with 3P-TOP. A549 cells have been transfected with respectively all fluorophore reporter plasmids and 3P-TOP. The amount of positively transfected cells is the average of 4 measurements. mT2+eGFP+tdT+iRFP transfected cells: 17,60 % of the cells signaled in the mT2 channel 40,40 % in the eGFP channel 29,10 % in the tdT and 4,42 % iRFP channel. 3P-TOP transfected cells: 7.08 % of the cells signaled in the mT2 channel 15,10 % in the eGFP channel 11,50 % in the tdT and 0,13 % iRFP channel

4.4 Transformation efficiencies of chemical and electrocompetent cells

The two protocols described in 3.7.1 and 3.7.2 were compared to estimate which one allow us to yield bacteria with a high transformation efficiency. Bacterial growth until catching the suggested OD_{600} is demonstrated in Figure 23. We used DH5α *E. coli* bacteria for most experiments, Stbl3 (also *E. coli*) have been used once just for comparison.

In the one attempt where Stbl3 were used, a transformation efficiency of $1,3*10^4$ was reached. Measured efficiency of DH5α prepared with method A was $1,3*10^5$. When method B was used an efficiency of $8,8*10^5$ was reached. The efficiency decreased about one potency ($7,5*10^4$) when measured only two days later, with cells kept at -80°C.

Transformation of electrocompetent cells led to better efficiencies: In total, we went for two attempts. We could reach following efficiencies:

4. First electroporation $2,92*10^7$ (mean value calculated out of the measurement of two dilutions 1:10 and 1:100)

5. Second electroporation $9,3*10^6$ (mean value calculated out of the measurement of two dilutions 1:10 and 1:100)
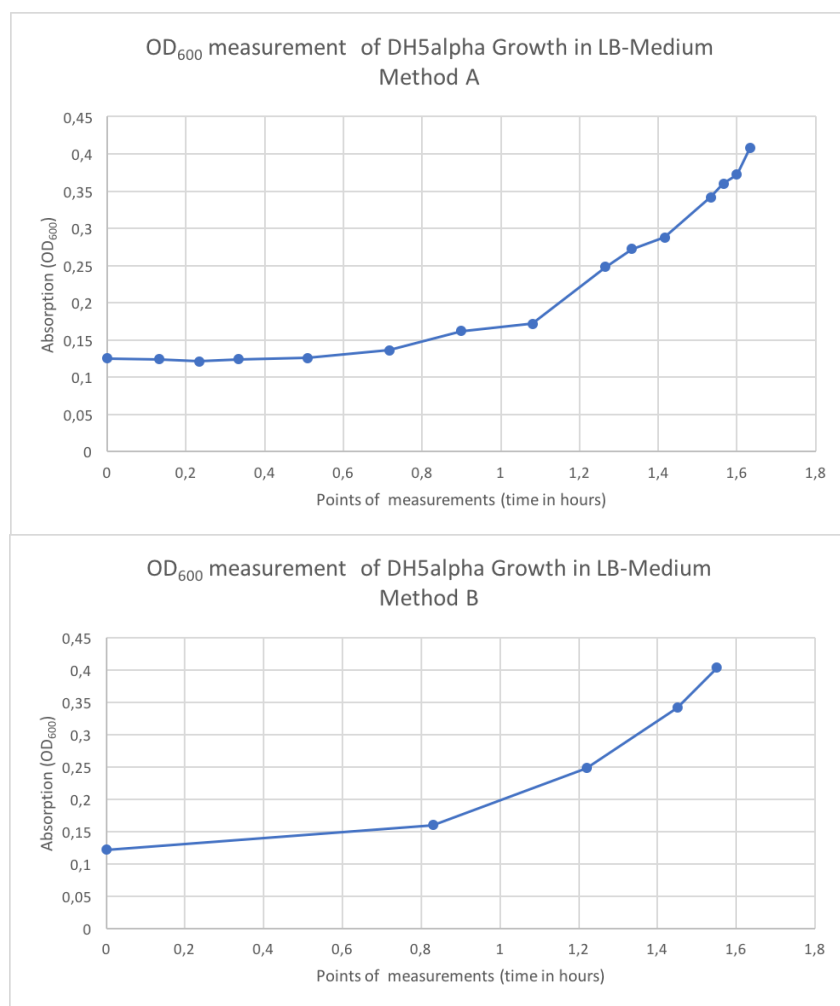
Figure 23 Bacterial growth in LB Medium in both methods for preparing chemical competent cells.

5 Discussion

5.1 Transfection

Before starting with the main experiments of the evaluation of the fluorophores EGFP, iRFP, mT2 and tdTomato via transfection we had to standardize our transfection method. As LPEI is potentially toxic for cells, we first had to experimentally determine the optimal conditions for the experiment. We decided to compare N/P 6 and N/P 9. Our results clearly showed that more cells were positively transfected by using a ratio of N/P 9 (Figure 15). When N/P 6 was used, 33,1% of the single cells were transfected, versus 38,1%when utilizing N/P 9. Therefore, we used N/P 9 for all following experiments.

5.2 Fluorescent reporter proteins experiments

We tried to exclude some confounding factors from the beginning. We did not use a viability stain because PI, DAPI and Hoechst are not suited for the 3P construct in flow cytometry, as their colours overlap with the reporter fluorophores (Figure 24). Hoechst
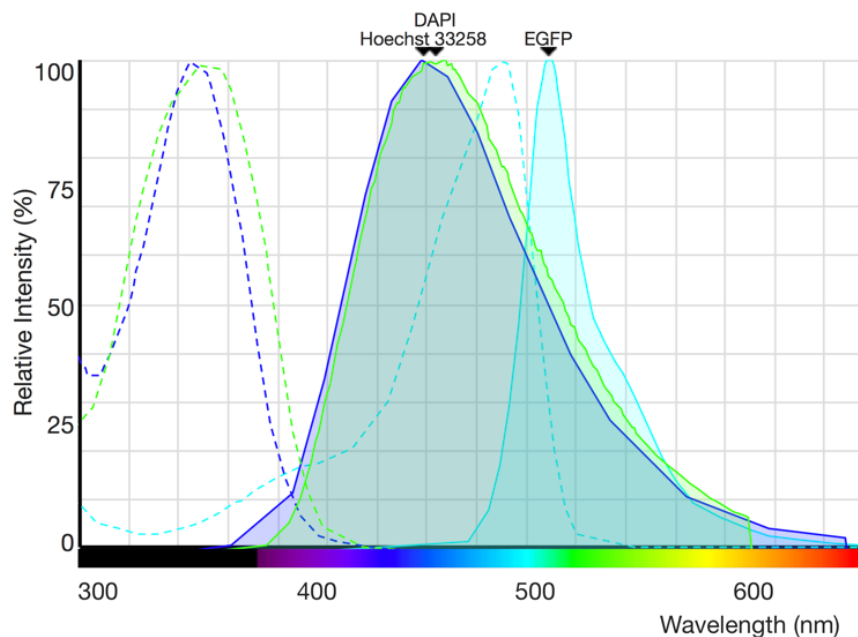
Figure 24 Excitation (dashed line) and emission spectra of viability stains DAPI and Hoechst compared to EGFP.
The green dashed line shows the excitation spectrum of DAPI and the continuous green line its emission spectrum. The overlap of the viability stains in the emission spectra is too high. The blue dashed line shows the excitation spectrum of Hoechst and the continuous blue line its emission spectrum. The overlap of the viability stains in the emission spectra is too high Therefore, we did not use any viability stain. Graph designed on the "Fluorescence SpectraViewer" provided by ThermoFisher Scientific (http://www.thermofisher.com/at/en/home/life-science/cell-analysis/labeling-chemistry/fluorescence-spectraviewer.html)

33342, DAPI and mTurquoise2 (ex: 434 nm, em: 474 nm) share the same excitation laser at 405 nm and the emission maxima (shown in Figure 24).

EGFP

EGFP – single transfection (Figure 20)

EGFP shines into the mT2 and tdT channel. That means when EGFP, mT2 and tdT are used at the same time in one experiment it is difficult to differentiate their emission spectra. This fact can lead to conflicting results. In our case, consider the following case: We try to test the activity of two pathways we could couple a fluorophore promoter on a specific pathway. Assume that a pathway A is coupled with EGFP and a pathway B is coupled with tdTomato. If A is active we get a signal in the EGFP channel. When checking the activity of pathway B also a signal is recognized in the tdTomato channel. As our results have shown that eGFP shines in the tdTomato channel and vice versa, as specific statement of pathway activities is not given. Moreover, more investigation is needed to see if the signal in the iRFP channel of 0,2% is negligible or not.

EGFP – co – transfections (Figure 21)

EGFP+iRFP

The expression of iRFP in the cell was very low in comparison with EGFP. Maybe the choice of the A549 cell line shows expression limitation of iRFP. The expression of all other fluorophores was relatively high compared to iRFP expression. This is explained when looking at the results: Always cells, which had been treated with iRFP showed a very small amount that shined into the iRFP channel.

EGFP+mT2:

Interference occurred in the tdT channel in~ 20% of the measured cells. So, this combination seems also to be unsuited for further experiments. Furthermore, from analysing the solo transfections of EGFP and mT2 (4.3) it is apparent that EGFP transfected cells shine in the mT2 channel and vice versa.

EGFP+tdTomato:

In this condition, the signal in the EGFP and tdT seems to be satisfying, if there would not be the interference described above in the solo transfection of EGFP. The signals in the

iRFP channel are less than 0,2% and in the mT2 channel less than 4% which could be neglected.

iRFP

iRFP – single transfection (Figure 20)

The cells transfected with iRFP showed very little events in the iRFP channel (Figure 15). Only ~ 19 % of the iRFP treated cells showed a signal. In other channels the signal was low: EGFP below 2%, mT2 below 0,7% and tdT below 0,4%. If these values could be neglected is unsure but iRFP shows a certain specificity as the most events have been measured in its own channel.

iRFP – co – transfections (Figure 21)

iRFP+mT2

The number of cells showed signal in the iRFP channel was very low but relatively high - ~ 27% - in the mT2 channel. Remarkable is the signal in the EGFP channel. The same quantity of cells gave signal in the mT2 gave signal in the EGFP channel. This underlines the interference between mT2 and EGFP (Figure 15).

iRFP+tdTomato

In my assessment, the results of this condition represent an outlier. Against expectation much more cells shined in the EGFP and mT2 channel (~ 20 and 30 %!) than in the iRFP and tdT channel. This occurrence should be investigated in further experiments.

mTurquoise2 (mT2)

mT2 – single transfection (Figure 20)

Like EGFP and tdT, mT2 also represents a problem fluorophore in our chosen set of fluorophores. ~ 30% of mT2 transfected cells showed signal in the EGFP channel and ~35% in the mT2 channel. In this regard, there is no specificity for the mT2 signal.

mT2+tdTomato

Nearly a quarter (~24%) of the transfected cells showed signal in every used channel except the iRFP channel. In connection from the solo transfection mT2 and tdT it could be derived that both, mT2 and tdT are responsible for the signal in EGFP channel.

tdTomato (tdT)

tdT – single transfection (Figure 20)

Like we've excepted tdT showed signal in the EGFP channel. ~ 40% of the cells gave signal in the EGFP channel and 30% in the tdT channel. This could be explained by the sharing of the emission wavelength spectrum between 519 – 615 nm (Figure 20).
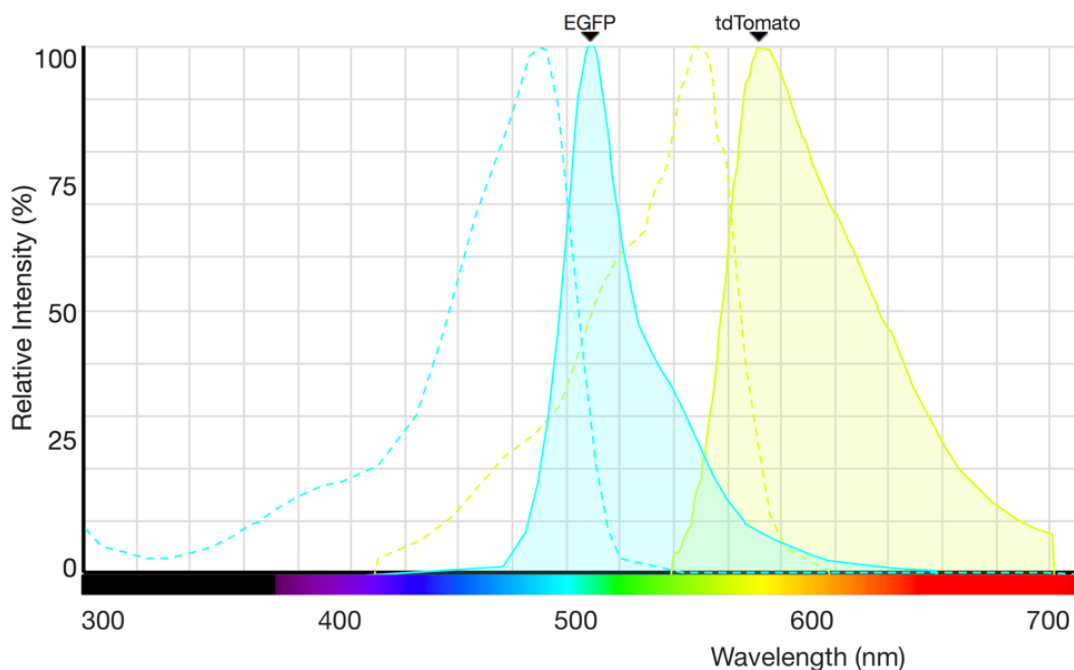
Figure 25 Excitation (dashed lines) and emission spectra of EGFP and tdTomato. A distinct overlap between EGFP emission (continuous cyan line) and tdTomato excitation (yellow dashed line)is shown. Graph designed on the "Fluorescence SpectraViewer" provided by ThermoFisher Scientific(http://www.thermofisher.com/at/en/home/life-science/cell-analysis/labeling-chemistry/fluorescence-spectraviewer.html

Moreover, the eGFP emission is overlapping with the excitation spectrum of tdTomato (~ 455-678 nm). That means that EGFP emission signal can excite tdTomato and so lead to false interpretations. This occurrence should be investigated in further experiments.

Co – Transfection of all Fluorophores together and 3P-TOP-transfection (Figure 22)

As shown in the results (Figure 17) there is signal in every fluorophore channel. Both conditions show low signal in the iRFP channel. For the 3P-TOP transfected cells an indeed

very low amount of 0,19% of cells gave signal in the iRFP channel. The signal resulted from the cells which have been transfected with all fluorophore reporters was by 4,4% of the cells. At this point it is to mention again that 3P-TOP is construct which has all genes that code for all evaluated fluorophores.

Summarizing our tested fluorophore proteins cannot be used for further experiments yet. The overlap problem of eGFP and tdTomato (Figure 25) could be solved by establishing a compensation matrix or even change one by another fluorophore. Also, mT2 did not show specificity in our experiments as it also gave signal in the EGFP channel. At this point I want to highlight that iRFP, in the matter of signalling in its channel, had the most speci-ficity but unfortunately very low expression level. I assume that the transfection worked well in every experiment. My suggestion of expression limitation of iRFP in A549 cells is based on the fact that it was the only fluorophore with low signal. Even in the 3P-TOP transfection the signal of all fluorophores was satisfying compared to iRFP. That supports my opinion of expression limits of iRFP by A549 cells. Hock et al. (2014) suggests among other cell lines HeLa cells as stably expressing iRFP. The choice of fluorophores must be tested in further in vitro experiments.

5.2.1 Compensation as the ideal approach

As explained in the introduction (1.3.1) compensation is a subtractive process what must be considered. Our results have clearly shown that we need to establish a compensation matrix in further experiments which enables us to use our fluorescent reporter proteins in multicolour experiments. The overlap of EGFP emission into the tdTomato spectrum is demonstrated in figure 25. For EGFP emission, the emission filters for B1: 525/50 nm and B2: 585/40 nm have been used and for tdTomato B2: 585/40 nm and B3-655-730 nm. The exact overlap within the filter spectra (same concept like shown in figure 9) must be eval-uated and so the amount of compensation which is required could be estimated. This con-cept must be adapted for each possible fluorescent duo combination we've done in this experiment. In order to see the amount of compensation which is required single colour samples are needed what in our case, we've achieved via expression of each fluorescent reporter proteins in A549 cells. This approach could so lead us to the possibility of using a broad range of fluorescent reporter proteins in multiparameter experiments regarding pro-motor related studies.

5.3 Preparation of competent cells

Preparation of chemical competent cells

The results of the comparison of method A and B to yield chemical competent cells were not satisfying. The fact that we have reached more than $x*10^5$ cfu/µg is challenging as a transformation efficiency of $1-3*10^9$ cfu/µg is recommended for example by Inoue (1990). Furthermore, it seemed that the maintenance of the transformation efficiency was problematic. We experienced a loss of competence. We went for several attempts and excluded sources of errors as good as we could but nevertheless didn't be able to get to satisfying results. As example, we've cooled all devices like seropipettes or pipette tips we've used. TB buffer was also always kept cooled. In some attempt, we also worked together and monitored each other for mistakes, excluding handling errors.

As the heat shock transformation which is performed in chemical competent cells is a reportedly simple and cheap method, we should assess other protocols for their performance. A suggestion is to maybe try the original Inoue protocol.

Preparation of electrocompetent cells

Electroporation was much more effective. Here we could get closer to the desired transformation efficiency (see 4.4). The method of preparing electrocompetent cells and following electroporation imply some advantages.
It is a very quick method and sources of errors are relatively low. After reaching the desired OD_{600} the cells have just been washed with ddH$_2$O. The only critical step is the electroporation itself. A complication is that the suspension which consists of the bacteria, the plasmid and ddH$_2$O must be deionized to avoid electrical shorts that lead to cell destruction. For example, when building a reporter construct in several steps the endproduct has to be additionally purified to remove all contaminations and ions in the batch. But this also has the disadvantage that a loss of plasmid will occur. Another disadvantage is that the for electroporation standardized cuvettes are expensive.

Altogether the choice of competent bacteria and subsequent transformation method must be well thought over. We should keep in mind that the preparation of chemical competent

cells and following heat shock transformation is a very cheap method and the preparation of electrocompetent cells and the following electroporation-transformation is expensive.

6 Appendix

6.1 Abstract

The cancer research field became increasingly relevant in the past decades. The understanding the character of a tumour is the base for a successful diagnosis and therapy of cancer.

Research has shown that three developmental pathways play a big role in tumorigenesis: The Hedgehog, Notch and Wnt pathways. The understanding of the function and activity of these pathways could lee to new approaches in fighting cancer.

A good method to visualize cellular mechanisms, like these pathways, is provided by fluorophores. As part of this thesis, four fluorophores were tested. The turquois fluorescing mTurquoise2, the green fluorescing eGFP, the red fluorescing tdTomato and the near infrared fluorescing iRFP. The aim is to eventually link this fluorophores to the mentioned pathways to get more clues about the functionality of these pathways in genesis of cancer. We have tested these fluorophore genes via transfection experiments with lung cancer cells. The behaviour of the fluorophores was evaluated via flow cytometry. In the end, we could figure out that the usage of these fluorophores in combination is not very practicable as they interference is too big. To evade this matter an establishment of a compensation matrix is recommended.

Another central topic in this thesis and in our laboratory, is the preparation of competent cells to get them easily transformable. Two protocols to prepare chemical competent cells and one protocol for preparing electrocompetent cells were tested. The competence of the bacteria was tested with the measurement of transformation efficiency. In our case the transformation efficiency when using electroporation was $2-3$ potencies higher compared to heat shock transformation of chemical competent cells. Moreover, we could find out that using electroporation to transform bacteria is a very quick method whereas the using of heat shock transformation of chemical competent cells takes much more time as the preparation of chemical competent cells is a very long process.

6.2 Zusammenfassung

In den letzten Jahrzenten die Krebsforschung immer mehr an Bedeutung gewonnen. Das Verständnis des Wesens eines Tumors stellt eine Grundlage für seine erfolgreiche Diagnose und Therapie dar.

Man konnte herausfinden, dass bei der Entstehung von Krebs drei Pathways oder auch biochemische Zellkaskaden eine große Rolle spielen. Der Hedgehog-, Notch- und Wnt-Pathway. Fehlregulierungen dieser Pathways tragen bei der Entstehung von Krebserkrankungen bei. Dahingehend besteht die Notwendigkeit einer Analyse dieser Pathways unter anderem über ihre Funktionsmechanismen und wodurch sie aktiviert werden und wann genau sie aktiv sind.

Eine einfache Methode um zelluläre Mechanismen zu visualisieren bieten fluoreszierenden Reporterproteine. Im Rahmen dieser Arbeit wurden vier Fluorophore ausgewertet. Das türkis fluoreszierende mTurquoise2, das grün fluoreszierende Protein eGFP, das rot fluoreszierende tdTomato und das nahe-infrarot fluoreszierende iRFP. Ziel ist es diese letztendlich an die Pathways zu koppeln sodass eine Aussage über ihre Aktivität ermöglicht werden kann. In unseren Experimenten wurde Krebszellen mit fluorophore-Genen transfeziert und ihr Emissionsverhalten mittels Durchflusszytometrie evaluiert. Unserer Resultate zeigten, dass aufgrund von Interferenzen, die Verwendung dieser Fluorophore in Kombination noch weitere Anforderungen benötigt, wie beispielsweise der Erstellung einer Kompensationsmatrix.

Ein anderes zentrales Thema dieser Arbeit und auch in unserem Labor ist die Vorbereitung von kompetenten Zellen um sie transformierbar zu machen. Zwei Protokolle, um sie chemisch kompetent zu machen und ein Protokoll, um sie elektrokompetent zu machen, wurden im Rahmen dieser Arbeit getestet. Inwiefern die Bakterien dann tatsächlich kompetent gemacht wurden, wurde mit einem Transformationseffizienztest ermittelt. Wir konnten herausfinden, dass in unserem Fall die Transformationseffizienz elektrokompetenter Zellen um $2-3$ Potenzen höher war, als jene der chemisch kompetenten Zellen. Zusätzlich konnten wir auch feststellen, dass die Transformation mittels Elektroporation viel schneller prozessiert werden kann als eine Hitzeschocktransformation, dahingehend, dass der Vorbereitung chemisch kompetenter Zellen ein großer Zeitaufwand beizumessen ist, wohingegen der Bereitung elektrokompetenter Zellen nicht.

7 References

Amakye, Dereck, Zainab Jagani, and Marion Dorsch. 2013. 'Unraveling the Therapeutic Potential of the Hedgehog Pathway in Cancer'. *Nature Medicine* 19 (11):1410–22. https://doi.org/10.1038/nm.3389.

Athar, Mohammad, Xiuwei Tang, Juliette L. Lee, Levy Kopelovich, and Arianna L. Kim. 2006. 'Hedgehog Signalling in Skin Development and Cancer'. *Experimental Dermatology* 15 (9):667–677.

Barrandon, Y., and H. Green. 1987. 'Three Clonal Types of Keratinocyte with Different Capacities for Multiplication'. *Proceedings of the National Academy of Sciences of the United States of America* 84 (8):2302–6.

Beachy, Philip A., Sarah G. Hymowitz, Robert A. Lazarus, Daniel J. Leahy, and Christian Siebold. 2010. 'Interactions between Hedgehog Proteins and Their Binding Partners Come into View'. *Genes & Development* 24 (18):2001–2012.

Beavis, Andrew J., and Robert F. Kalejta. 1999. 'Simultaneous Analysis of the Cyan, Yellow and Green Fluorescent Proteins by Flow Cytometry Using Single-Laser Excitation at 458 Nm'. *Cytometry* 37 (1):68–73.

Beck, Benjamin, and Cédric Blanpain. 2013. 'Unravelling Cancer Stem Cell Potential'. *Nature Reviews. Cancer* 13 (10):727.

Behrens, Jürgen. 2000. 'Control of β-Catenin Signaling in Tumor Development'. *Annals of the New York Academy of Sciences* 910 (1):21–35.

Bishop, J. Michael, and Robert Allan Weinberg. 1996. *Scientific American Molecular Oncology*. Scientific American.

Boeckle, Sabine, Katharina von Gersdorff, Silke van der Piepen, Carsten Culmsee, Ernst Wagner, and Manfred Ogris. 2004. 'Purification of Polyethylenimine Polyplexes Highlights the Role of Free Polycations in Gene Transfer'. *The Journal of Gene Medicine* 6 (10):1102–1111.

Brown, Maureen D., Andreas G. Schätzlein, and Ijeoma F. Uchegbu. 2001. 'Gene Delivery with Synthetic (Non Viral) Carriers'. *International Journal of Pharmaceutics* 229 (1):1–21.

Burnell, Elliott, Loek Van Alphen, Arie Verkleij, and Ben De Kruijff. 1980. '31P Nuclear Magnetic Resonance and Freeze-Fracture Electron Microscopy Studies on Escherichia Coli. I. Cytoplasmic Membrane and Total Phospholipids'. *Biochimica et Biophysica Acta (BBA)- Biomembranes* 597 (3):492–501.

Cancer Research UK. 2015. 'Worldwide Cancer Statistics'. Cancer Research UK. 13 May 2015. http://www.cancerresearchuk.org/health-professional/cancer-statistics/worldwide-cancer.

Chalfie, Martin, Yuan Tu, Ghia Euskirchen, William W. Ward, and Douglas C. Prasher. 1994.

'Green Fluorescent Protein as a Marker for Gene Expression'. *Science*, 802–805.

Chan, Weng-Tat, Chandra S. Verma, David P. Lane, and Samuel Ken-En Gan. 2013. 'A Comparison and Optimization of Methods and Factors Affecting the Transformation of Escherichia Coli'. *Bioscience Reports* 33 (6). https://doi.org/10.1042/BSR20130098.

Chang, Roger L., Kathleen Andrews, Donghyuk Kim, Zhanwen Li, Adam Godzik, and Bernhard O. Palsson. 2013. 'Structural Systems Biology Evaluation of Metabolic Thermotolerance in Escherichia Coli'. *Science* 340 (6137):1220–1223.

Chen, Ellson Y., and Peter H. Seeburg. 1985. 'Supercoil Sequencing: A Fast and Simple Method for Sequencing Plasmid DNA'. *Dna* 4 (2):165–170.

Chung, C. T., Suzanne L. Niemela, and Roger H. Miller. 1989. 'One-Step Preparation of Competent Escherichia Coli: Transformation and Storage of Bacterial Cells in the Same Solution'. *Proceedings of the National Academy of Sciences* 86 (7):2172–2175.

Clarke, Michael F., John E. Dick, Peter B. Dirks, Connie J. Eaves, Catriona HM Jamieson, D. Leanne Jones, Jane Visvader, Irving L. Weissman, and Geoffrey M. Wahl. 2006. 'Cancer Stem Cells—perspectives on Current Status and Future Directions: AACR Workshop on Cancer Stem Cells'. *Cancer Research* 66 (19):9339–9344.

Clevers, Hans. 2011. 'The Cancer Stem Cell: Premises, Promises and Challenges'. *Nature Medicine*, 313–319.

Cormack, Brendan P., Raphael H. Valdivia, and Stanley Falkow. 1996. 'FACS-Optimized Mutants of the Green Fluorescent Protein (GFP)'. *Gene* 173 (1):33–38.

De Laporte, Laura, Jennifer Cruz Rea, and Lonnie D. Shea. 2006. 'Design of Modular Non-Viral Gene Therapy Vectors'. *Biomaterials* 27 (7):947–954.

Dexter, Daniel L., Henryk M. Kowalski, Beverly A. Blazar, Zuzana Fligiel, Renee Vogel, and Gloria H. Heppner. 1978. 'Heterogeneity of Tumor Cells from a Single Mouse Mammary Tumor'. *Cancer Research* 38 (10):3174–3181.

Dick, John E. 2008. 'Stem Cell Concepts Renew Cancer Research'. *Blood* 112 (13):4793–4807.

Dower, William J., Jeff F. Miller, and Charles W. Ragsdale. 1988. 'High Efficiency Transformation of E. Coli by High Voltage Electroporation'. *Nucleic Acids Research* 16 (13):6127–6145.

Dunlap, David D., Alessia Maggi, Marco R. Soria, and Lucia Monaco. 1997. 'Nanoscopic Structure of DNA Condensed for Gene Delivery'. *Nucleic Acids Research* 25 (15):3095–3101.

Espinoza, Ingrid, and Lucio Miele. 2013. 'Notch Inhibitors for Cancer Treatment'. *Pharmacology & Therapeutics* 139 (2):95–110. https://doi.org/10.1016/j.pharmthera.2013.02.003.

'FDA Approval for Vismodegib'. n.d. CgvArticle. National Cancer Institute. Accessed 3 November 2017. https://www.cancer.gov/about-cancer/treatment/drugs/fda-vismodegib.

Filonov, Grigory S., Kiryl D. Piatkevich, Li-Min Ting, Jinghang Zhang, Kami Kim, and Vladislav V. Verkhusha. 2011. 'Bright and Stable Near-Infrared Fluorescent Protein for in Vivo Imaging'. *Nature Biotechnology* 29 (8):757–761.

Gao, Chan, and Ye-Guang Chen. 2010. 'Dishevelled: The Hub of Wnt Signaling'. *Cellular Signalling* 22 (5):717–727.

Gardam, Michael A., Edward C. Keystone, Richard Menzies, Steven Manners, Emil Skamene, Richard Long, and Donald C. Vinh. 2003. 'Anti-Tumour Necrosis Factor Agents and Tuberculosis Risk: Mechanisms of Action and Clinical Management'. *The Lancet. Infectious Diseases* 3 (3):148–55.

Gerritsen, W. J., B. De Kruijff, A. J. Verkleij, J. De Gier, and L. L. M. Van Deenen. 1980. 'Ca2+-Induced Isotropic Motion and Phosphatidylcholine Flip-Flop in Phosphatidylcholine-Cardiolipin Bilayers'. *Biochimica et Biophysica Acta (BBA)-Biomembranes* 598 (3):554–560.

Godbey, W. T., Kenneth K. Wu, and Antonios G. Mikos. 1999. 'Poly (Ethylenimine) and Its Role in Gene Delivery'. *Journal of Controlled Release* 60 (2):149–160.

Goedhart, Joachim, David Von Stetten, Marjolaine Noirclerc-Savoye, Mickaël Lelimousin, Linda Joosen, Mark A. Hink, Laura Van Weeren, Theodorus WJ Gadella Jr, and Antoine Royant. 2012. 'Structure-Guided Evolution of Cyan Fluorescent Proteins towards a Quantum Yield of 93%'. *Nature Communications* 3:751.

Gómez-del Arco, Pablo, Mariko Kashiwagi, Audrey F. Jackson, Taku Naito, Jiangwen Zhang, Feifei Liu, Barbara Kee, et al. 2010. 'Alternative Promoter Usage at the Notch1 Locus Supports Ligand-Independent Signaling in T Cell Development and Leukemogenesis'. *Immunity* 33 (5):685–98. https://doi.org/10.1016/j.immuni.2010.11.008.

Gu, Jian-Wei, Paola Rizzo, Antonio Pannuti, Todd Golde, Barbara Osborne, and Lucio Miele. 2012. 'Notch Signals in the Endothelium and Cancer "Stem-like" Cells: Opportunities for Cancer Therapy'. *Vascular Cell* 4 (1):7. https://doi.org/10.1186/2045-824X-4-7.

Habas, Raymond, and Igor B. Dawid. 2005. 'Dishevelled and Wnt Signaling: Is the Nucleus the Final Frontier?' *Journal of Biology* 4 (1):2.

Hanahan, Douglas. 1983. 'Studies on Transformation of Escherichia Coli with Plasmids'. *Journal of Molecular Biology* 166 (4):557–580.

Hanahan, Douglas, and Robert A. Weinberg. 2000. 'The Hallmarks of Cancer'. *Cell* 100 (1):57–70.

Hanahan, Douglas, and Robert A. Weinberg. 2011. 'Hallmarks of Cancer: The Next Generation'. *Cell* 144 (5):646–74. https://doi.org/10.1016/j.cell.2011.02.013.

Hawley, Teresa S., Donald J. Herbert, Shannon S. Eaker, and Robert G. Hawley. 2004. 'Multiparameter Flow Cytometry of Fluorescent Protein Reporters'. *Flow Cytometry Protocols*, 219–237.

Heim, Roger, Douglas C. Prasher, and Roger Y. Tsien. 1994. 'Wavelength Mutations and Posttranslational Autoxidation of Green Fluorescent Protein'. *Proceedings of the National Academy of Sciences* 91 (26):12501–12504.

Hock, Andreas K., Pearl Lee, Oliver DK Maddocks, Susan M. Mason, Karen Blyth, and Karen H. Vousden. 2014. 'IRFP Is a Sensitive Marker for Cell Number and Tumor Growth in High-Throughput Systems'. *Cell Cycle* 13 (2):220–26. https://doi.org/10.4161/cc.26985.

Hope, Kristin J., Liqing Jin, and John E. Dick. 2004. 'Acute Myeloid Leukemia Originates from a Hierarchy of Leukemic Stem Cell Classes That Differ in Self-Renewal Capacity'. *Nature Immunology* 5 (7):738–43. https://doi.org/10.1038/ni1080.

Huang, Shih-Min A., Yuji M. Mishina, Shanming Liu, Atwood Cheung, Frank Stegmeier, Gregory A. Michaud, Olga Charlat, et al. 2009. 'Tankyrase Inhibition Stabilizes Axin and Antagonizes Wnt Signalling'. *Nature* 461 (7264):614–20. https://doi.org/10.1038/nature08356.

'Infinity Stops Phase 2 Trials of Saridegib in Chondrosarcoma and Myelofibrosis'. 2012. 18 June 2012. http://www.businesswire.com/news/home/20120618005411/en/Infinity-Stops-Phase-2-Trials-Saridegib-Chondrosarcoma.

Inoue, Hiroaki, Hiroshi Nojima, and Hiroto Okayama. 1990. 'High Efficiency Transformation of Escherichia Coli with Plasmids'. *Gene* 96 (1):23–28.

Jin, Lian, Xin Zeng, Ming Liu, Yan Deng, and Nongyue He. 2014. 'Current Progress in Gene Delivery Technology Based on Chemical Methods and Nano-Carriers'. *Theranostics* 4 (3):240.

Karamboulas, Christina, and Laurie Ailles. 2013. 'Developmental Signaling Pathways in Cancer Stem Cells of Solid Tumors'. *Biochimica Et Biophysica Acta* 1830 (2):2481–95. https://doi.org/10.1016/j.bbagen.2012.11.008.

Kawakami, Shigeru, Yoshitaka Ito, Pensri Charoensit, Fumiyoshi Yamashita, and Mitsuru Hashida. 2006. 'Evaluation of Proinflammatory Cytokine Production Induced by Linear and Branched Polyethylenimine/Plasmid DNA Complexes in Mice'. *Journal of Pharmacology and Experimental Therapeutics* 317 (3):1382–1390.

Kreso, Antonija, and John E. Dick. 2014. 'Evolution of the Cancer Stem Cell Model'. *Cell Stem Cell* 14 (3):275–91. https://doi.org/10.1016/j.stem.2014.02.006.

Lecoq, Jérôme, and Mark J. Schnitzer. 2011. 'An Infrared Fluorescent Protein for Deeper Imaging'. *Nature Biotechnology* 29 (8):715–716.

Lee, Ho-Jin, Nick X. Wang, De-Li Shi, and Jie J. Zheng. 2009. 'Sulindac Inhibits Canonical Wnt Signaling by Blocking the PDZ Domain of the Protein Dishevelled'. *Angewandte Chemie International Edition* 48 (35):6448–52. https://doi.org/10.1002/anie.200902981.

Matz, Mikhail V., Arkady F. Fradkov, Yulii A. Labas, Aleksandr P. Savitsky, Andrey G. Zaraisky, Mikhail L. Markelov, and Sergey A. Lukyanov. 1999. 'Fluorescent Proteins from Nonbioluminescent Anthozoa Species'. *Nature Biotechnology* 17 (10):969–973.

Moghimi, S. Moein, Peter Symonds, J. Clifford Murray, A. Christy Hunter, Grazyna Debska, and Adam Szewczyk. 2005. 'A Two-Stage Poly (Ethylenimine)-Mediated Cytotoxicity: Implications for Gene Transfer/Therapy'. *Molecular Therapy* 11 (6):990–995.

Neumann, Eberhard, G. Gerisch, and K. Opatz. 1980. 'Cell Fusion Induced by High Electric Impulses Applied to Dictyostelium'. *Naturwissenschaften* 67 (8):414–415.

Neumann, Eberhard, and Kurt Rosenheck. 1972. 'Permeability Changes Induced by Electric Impulses in Vesicular Membranes'. *The Journal of Membrane Biology* 10 (1):279–90. https://doi.org/10.1007/BF01867861.

Nguyen, Long V., Robert Vanner, Peter Dirks, and Connie J. Eaves. 2012. 'Cancer Stem Cells: An Evolving Concept'. *Nature Reviews. Cancer* 12 (2):133.

Nimesh, Surendra, Anita Aggarwal, Pradeep Kumar, Yogendra Singh, K. C. Gupta, and Ramesh Chandra. 2007. 'Influence of Acyl Chain Length on Transfection Mediated by Acylated PEI Nanoparticles'. *International Journal of Pharmaceutics* 337 (1):265–274.

Nowell, Peter C. 1976. 'The Clonal Evolution of Tumor Cell Populations'. *Science* 194 (4260):23–28.

Odoux, C., H. Fohrer, T. Hoppo, L. Guzik, D. B. Stolz, D. W. Lewis, S. M. Gollin, T. C. Gamblin, D. A. Geller, and E. Lagasse. 2008. 'A Stochastic Model for Cancer Stem Cell Origin in Metastatic Colon Cancer'. *Cancer Research* 68 (17):6932–41. https://doi.org/10.1158/0008-5472.CAN-07-5779.

Ormo, Mats, Andrew B. Cubitt, Karen Kallio, and Larry A. Gross. 1996. 'Crystal Structure of the Aequorea Victoria Green Fluorescent Protein'. *Science* 273 (5280):1392.

Palma, Verónica, Daniel A. Lim, Nadia Dahmane, Pilar Sánchez, Thomas C. Brionne, Claudia D. Herzberg, Yorick Gitton, Alan Carleton, Arturo Álvarez-Buylla, and Ariel Ruiz i Altaba. 2005. 'Sonic Hedgehog Controls Stem Cell Behavior in the Postnatal and Adult Brain'. *Development* 132 (2):335–344.

Panja, Subrata, Swati Saha, Bimal Jana, and Tarakdas Basu. 2006. 'Role of Membrane Potential on Artificial Transformation of E. Coli with Plasmid DNA'. *Journal of Biotechnology* 127 (1):14–20.

Pertschuk, Louis P., Ellis H. Tobin, David J. Brigati, Dong S. Kim, Norman D. Bloom, Eric Gaetjens, Peter J. Berman, Anne C. Carter, and George A. Degenshein. 1978. 'Immunofluorescent Detection of Estrogen Receptors in Breast Cancer. Comparison with Dextran-Coated Charcoal and Sucrose Gradient Assays'. *Cancer* 41 (3):907–911.

Pierce, G. B., F. J. Dixon, and E. Verney. 1959. 'Testicular Teratomas. I. Demonstration of Teratogenesis by Metamorphosis of Multipotential Cells'. *Cancer* 12 (3):573–583.

Pierce, G. B., F. J. Dixon, and E. L. Verney. 1960. 'Teratocarcinogenic and Tissue-Forming Potentials of the Cell Types Comprising Neoplastic Embryoid Bodies'. *Laboratory Investigation; a Journal of Technical Methods and Pathology* 9 (December):583–602.

Poste, G., J. Doll, I. R. Hart, and I. J. Fidler. 1980. 'In Vitro Selection of Murine B16 Melanoma Variants with Enhanced Tissue-Invasive Properties'. *Cancer Research* 40 (5):1636–1644.

Prakash, G. Divya, R. V. Anish, G. Jagadeesh, and Dipshikha Chakravortty. 2011. 'Bacterial Transformation Using Micro-Shock Waves'. *Analytical Biochemistry* 419 (2):292–301.

Quintana, Elsa, Mark Shackleton, Hannah R. Foster, Douglas R. Fullen, Michael S. Sabel,

Timothy M. Johnson, and Sean J. Morrison. 2010. 'Phenotypic Heterogeneity among Tumorigenic Melanoma Cells from Patients That Is Reversible and Not Hierarchically Organized'. *Cancer Cell* 18 (5):510–523.

Quintana, Elsa, Mark Shackleton, Michael S. Sabel, Douglas R. Fullen, Timothy M. Johnson, and Sean J. Morrison. 2008. 'Efficient Tumor Formation by Single Human Melanoma Cells'. *Nature* 456 (7222):593.

Rahimzadeh, Maral, Majid Sadeghizadeh, Farhood Najafi, Seyed Arab, and Hamid Mobasheri. 2016. 'Impact of Heat Shock Step on Bacterial Transformation Efficiency'. *Molecular Biology Research Communications* 5 (4):257–61.

Raz, A., W. L. McLellan, I. R. Hart, C. D. Bucana, L. C. Hoyer, B. A. Sela, P. Dragsten, and I. J. Fidler. 1980. 'Cell Surface Properties of B16 Melanoma Variants with Differing Metastatic Potential'. *Cancer Research* 40 (5):1645–1651.

Schaffert, David, Christina Troiber, and Ernst Wagner. 2012. 'New Sequence-Defined Polyaminoamides with Tailored Endosomolytic Properties for Plasmid DNA Delivery'. *Bioconjugate Chemistry* 23 (6):1157–1165.

Shaner, Nathan C, Robert E Campbell, Paul A Steinbach, Ben N G Giepmans, Amy E Palmer, and Roger Y Tsien. 2004. 'Improved Monomeric Red, Orange and Yellow Fluorescent Proteins Derived from Discosoma Sp. Red Fluorescent Protein'. *Nature Biotechnology* 22 (12):1567–72. https://doi.org/10.1038/nbt1037.

Shaner, Nathan C., George H. Patterson, and Michael W. Davidson. 2007. 'Advances in Fluorescent Protein Technology'. *Journal of Cell Science* 120 (24):4247–4260.

Shaner, Nathan C., Paul A. Steinbach, and Roger Y. Tsien. 2005. 'A Guide to Choosing Fluorescent Proteins'. *Nature Methods* 2 (12):905.

Shimomura, Osamu, Frank H. Johnson, and Yo Saiga. 1962. 'Extraction, Purification and Properties of Aequorin, a Bioluminescent Protein from the Luminous Hydromedusan, Aequorea'. *Journal of Cellular Physiology* 59 (3):223–239.

Smith, David C., Lee S. Rosen, Rashmi Chugh, Jonathan Wade Goldman, Lu Xu, Ann Kapoun, Ranier K. Brachmann, et al. 2013. 'First-in-Human Evaluation of the Human Monoclonal Antibody Vantictumab (OMP-18R5; Anti-Frizzled) Targeting the WNT Pathway in a Phase I Study for Patients with Advanced Solid Tumors'. *J. Clin. Oncol* 31 (15 Suppl). http://www.oncomed.com/presentations/Vantictumab_Ph1_ASCO%202013.pdf.

Stanton, Benjamin Z., Lee F. Peng, Nicole Maloof, Kazuo Nakai, Xiang Wang, Jay L. Duffner, Kennedy M. Taveras, et al. 2009. 'A Small Molecule That Binds Hedgehog and Blocks Its Signaling in Human Cells'. *Nature Chemical Biology* 5 (3):154–56. https://doi.org/10.1038/nchembio.142.

Statistics Austria. 2017. 'Cancer Incidence'. 22 February 2017. http://www.statistik.at/web_en/statistics/PeopleSociety/health/cancer_incidence/index.html.

Sugar, Istvan P., and Eberhard Neumann. 1984. 'Stochastic Model for Electric Field-Induced Membrane Pores Electroporation'. *Biophysical Chemistry* 19 (3):211–225.

Takebe, Naoko, Lucio Miele, Pamela Jo Harris, Woondong Jeong, Hideaki Bando, Michael Kahn, Sherry X. Yang, and S. Percy Ivy. 2015. 'Targeting Notch, Hedgehog, and Wnt Pathways in Cancer Stem Cells: Clinical Update'. *Nature Reviews Clinical Oncology* 12 (8):445–64. https://doi.org/10.1038/nrclinonc.2015.61.

Taylor, Robin G., David C. Walker, and R. R. McInnes. 1993. 'E. Coli Host Strains Significantly Affect the Quality of Small Scale Plasmid DNA Preparations Used for Sequencing.' *Nucleic Acids Research* 21 (7):1677.

ThermoFischer. n.d. 'GeneJET Plasmid Maxiprep Kit - Thermo Fisher Scientific'. Accessed 18 October 2017. https://www.thermofisher.com/order/catalog/product/K0491.

Torre, Lindsey A., Freddie Bray, Rebecca L. Siegel, Jacques Ferlay, Joannie Lortet-Tieulent, and Ahmedin Jemal. 2015. 'Global Cancer Statistics, 2012'. *CA: A Cancer Journal for Clinicians* 65 (2):87–108. https://doi.org/10.3322/caac.21262.

Tsien, Roger Y. 1998. *The Green Fluorescent Protein*. Annual Reviews 4139 El Camino Way, PO Box 10139, Palo Alto, CA 94303-0139, USA.

Van Die, Irma M., Hans EN Bergmans, and Wiel PM Hoekstra. 1983. 'Transformation in Escherichia Coli: Studies on the Role of the Heat Shock in Induction of Competence'. *Microbiology* 129 (3):663–670.

Verkleij, A. J., B. De Kruyff, PHJ Th Ververgaert, J. F. Tocanne, and L. L. M. Van Deenen. 1974. 'The Influence of PH, Ca2+ and Protein on the Thermotropic Behaviour of the Negatively Charged Phospholipid, Phosphatidylglycerol'. *Biochimica et Biophysica Acta (BBA)-Biomembranes* 339 (3):432–437.

Vu, Lucas, James Ramos, Thrimoorthy Potta, and Kaushal Rege. 2012. 'Generation of a Focused Poly (Amino Ether) Library: Polymer-Mediated Transgene Delivery and Gold-Nanorod Based Theranostic Systems'. *Theranostics* 2 (12):1160.

Waaler, J., O. Machon, L. Tumova, H. Dinh, V. Korinek, S. R. Wilson, J. E. Paulsen, et al. 2012. 'A Novel Tankyrase Inhibitor Decreases Canonical Wnt Signaling in Colon Carcinoma Cells and Reduces Tumor Growth in Conditional APC Mutant Mice'. *Cancer Research* 72 (11):2822–32. https://doi.org/10.1158/0008-5472.CAN-11-3336.

Yin, Tao, Guoping Wang, Tinghong Ye, and Yongsheng Wang. 2016. 'Sulindac, a Non-Steroidal Anti-Inflammatory Drug, Mediates Breast Cancer Inhibition as an Immune Modulator'. *Scientific Reports* 6 (1). https://doi.org/10.1038/srep19534.

Zhang, Bo, Xinpeng Ma, William Murdoch, Maciej Radosz, and Youqing Shen. 2013. 'Bioreducible Poly (Amido Amine) s with Different Branching Degrees as Gene Delivery Vectors'. *Biotechnology and Bioengineering* 110 (3):990–998.

Zimmermann, Ulrich, Peter Scheurich, Günter Pilwat, and Roland Benz. 1981. 'Cells with Manipulated Functions: New Perspectives for Cell Biology, Medicine, and Technology'. *Angewandte Chemie International Edition* 20 (4):325–344.

Zou, Shao-Min, Patrick Erbacher, Jean-Serge Remy, and Jean-Paul Behr. 2000. 'Systemic Linear Polyethylenimine (L-PEI)-Mediated Gene Delivery in the Mouse'. *The Journal of Gene Medicine* 2 (2):128–134.